Spring 2019

Design and Manufacture of an Inertial Cascade Impactor for Industrial Hygiene Purposes

Hector Joel Gortaire
Old Dominion University

DESIGN AND MANUFACTURE OF AN INERTIAL CASCADE IMPACTOR

FOR INDUSTRIAL HYGIENE PURPOSES

by

Hector Joel Gortaire
B.S. May 2016, Old Dominion University

A Thesis Submitted to the Faculty of
Old Dominion University in Partial Fulfillment of the
Requirements for the Degree of

MASTER OF SCIENCE

AEROSPACE ENGINEERING

OLD DOMINION UNIVERSITY

April 2019

Approved by:

Shizhi Qian (Director)

Venkat Maruthamuthu (Member)

Xiaoyu Zhang (Member)

ABSTRACT

DESIGN AND MANUFACTURE OF AN INERTIAL CASCADE IMPACTOR
FOR INDUSTRIAL HYGIENE PURPOSES

Hector Joel Gortaire

Old Dominion University, 2019

Director: Dr. Shizhi Qian

Inertial cascade impactors are devices commonly used for industrial hygiene and pharmaceutical studies. Their main purpose is to separate particulate matter suspended in aerosols according to their sizes, which can vary from over 10 µm to 0.5 µm. Their versatility and ease of operation make them suitable for on-site sampling; however, designing them requires a careful consideration of the different geometric parameters that characterize them.

In this thesis, a 5-stage inertial cascade impactor was designed, modelled, constructed, and tested. The main design parameter was the volumetric flow rate, 40 l/min, which was provided by a vacuum pump. By continuous iterations, it was possible to determine the number of nozzles, and their diameters at each stage, so that the calculated Reynolds number was as close to 3,000 as possible. It was also critical to keep the ratios $\frac{S}{W} = 1$ and $1 \leq \frac{T}{W} \leq 5$; where S represents the distance between the end of the nozzle (also known as jet) to the collection plate in each stage, T represents the nozzle throat length, and W represents the diameter of the circular nozzle.

These stages (1 through 5) were designed so that their cutoff diameters were 10, 5, 2, 1, and 0.5 µm, respectively. Due to the complexity of the air flow within the inertial cascade

impactor, the flow field of the designed cascade impactor was numerically simulated by a turbulent kinetic epsilon 2D-flow model in a stationary study, using the commercial finite element package COMSOL. The numerical results provided an insight on the behavior of the aerosol as it flows through it. After the cascade impactor was constructed, it was tested taking a 24-hour and a 60-hour air samples. Its performance was further characterized by analyzing the mass and size of the collected samples on each stage of the impactor. The numerical and experimental results show satisfactory agreement with the predicted behavior of this cascade impactor.

This thesis is dedicated to my mom Aura for setting the example for me to follow,

and to my wife Fanny for her unwavering love and support.

ACKNOWLEDGMENTS

I want to express my deepest gratitude to my thesis director, Dr. Qian, for his relentless guidance throughout the development of my thesis. Additionally, I want to thank the board members, Dr Maruthamuthu and Dr. Zhang for their invaluable support.

NOMENCLATURE

PM Particulate matter

ρ Air density

μ Air dynamic viscosity

ν Air kinematic viscosity

ψ Stream function

ψ' Nondimensional stream function

$\vec{\zeta}$ Vorticity

Re Reynolds number

W Nozzle diameter

$\dot{Q}$ Volumetric flow rate

S Distance between the end of the nozzle to the collection plate in each stage

T Nozzle throat length

Q Total volumetric flow rate

ρ_p Pparticle density

Stk_{50} Stokes number at 50% efficiency in one stage

n Number of nozzles in a stage

$\sqrt{C}$ Cunningham slip correction factor

D_{50} Equivalent aerodynamic radius of a unit density sphere

D_p Diameter of particle

V_0 Air velocity within nozzle

Table   Page

LIST OF FIGURES

TABLE OF CONTENTS

Chapter

INTRODUCTION

INERTIAL CASCADE IMPACTORS

5-STAGE INERTIAL CASCADE IMPACTOR DESIGN

EXPERIMENTS

CONCLUSIONS AND FUTURE WORK

Appendix

CHAPTER 1

INTRODUCTION

1.1 Behavior of particulate matter in the respiratory system.

The human respiratory apparatus has evolved throughout millions of years to function in dust-laden environments. The atmosphere contains airborne organic and inorganic particulate matter, which is continuously breathed in by all living creatures on earth. In order to adapt to this inevitable living condition, lungs have developed several mechanisms to prevent damage to tissue and protect humans from disease and death.

The main mission of these mechanisms of protection is to block and remove any particles that may cause damage to the respiratory apparatus, before they reach important and delicate parts and tissue. Among these mechanisms are the mucociliary escalator and the macrophage system which remove dust particles. Additionally, dead and damaged lung cells can be quickly replaced, which helps maintain a healthy and functional respiratory apparatus.

Despite these protective measures, overexposure to dust-laden environments could cause a collapse on these natural protection mechanisms. This overexposure could be the result of high concentration of organic or inorganic particulate matter in the air, or a prolonged exposure to environments with low but constant concentration of these particles. Many factors are present in the process of breathing in dust particles; for instance, the chemical composition of these particles and their physical nature. Clayton and Clayton (1991), state that the dose of inorganic particulate matter absorbed by the lungs is related to the biological response of the respiratory apparatus. Another important factor is the level of exposure to respirable particles in the occupational environment. A worker exposed to high concentration of airborne microscopic

debris has higher chances of breathing it in, if not equipped with the appropriate respiratory personal protective equipment.

During the process of breathing, air and the particulate matter contained in it pass through each of the main bronchi that lead to each lung. Clayton and Clayton (1991) state that these bronchi branch out in approximately 116,300 smaller limbs and twigs, which provide an extremely high probability of the particles contained in each breath to impinge on them before reaching further into the 300 million alveoli contained in the lungs. Consequently, the particles that impinge on the bronchi ramifications are removed by the mucociliary escalator mechanism which moves them away towards the mouth where they are expelled by coughing or swallowed; however, it is logical to accept that not all particles are expelled from the lungs, and some smaller particles reach the innermost regions of the lungs.

Besides, Clayton and Clayton (1991) mention that the sizes of the particles that can be found deposited in the lungs of a worker exposed to "dusty trades" have specific ranges: Approximately half of them have a diameter smaller than 0.5 µm; the diameter of another large amount of them ranges between 0.5 and 5 µm. Besides, less than 0.2% have a diameter greater than 5 µm, and less than 0.002% have a diameter larger than 10 µm. This distribution of particles deposited in the lungs is the result of the physics of the airflow into them. As air is drawn into the respiratory system, the particles suspended in it have the same velocity as the stream. When the breathed-in air column reaches the nose cavity, and changes direction within it, inertia forces the particles to keep their direction which causes them to hit the internal walls of the nasal cavity. This process repeats continuously within the respiratory system branches.

The impingement of particles within the walls of the respiratory system is directly proportional to the particle sizes and the air stream speed; and inversely proportional to the local radius of the

cross-section of the cavity through which the airstream flows. Another important factor that contributes to the impingement of particles is gravity, which causes precipitation of these particles on the surfaces of the respiratory system. The velocity with which particles settle down in the respiratory system is called terminal settling velocity, and it is proportional to the particle density, the square root of the particle diameter (assuming spherical shape), and gravity; it is inversely proportional to the air viscosity.

Experiments show that particles of diameter greater than 10 µm are removed at the nose cavity and higher airways; particles with a diameter range between 5 and 10 µm deposit on the upper airways of the mucociliary escalator. Particles of diameter range between 1 and 2 µm penetrate the innermost parts of the lungs where the main factors that cause precipitation of these particles are gravity and diffusion. Particles with diameter smaller than 0.5 µm and mainly smaller than 0.1 µm diffuse into the respiratory system surface.

The need to determine the contents and size distribution of particulate matter in an aerosol for air sampling purposes, led to the development of several methods to accomplish this, and the design of several devices. Cascade impactors are an example of these devices. They work under a principle similar to the precipitation of particulate matter within the respiratory system surface.

The use of cascade impactors in air sampling helps determine the distribution of particulate matter in aerosols, which can adversely affect the respiratory apparatus normal functioning and lead to illness or death. This is important when studying air pollution; and besides, sound industrial hygiene practices should eliminate or reduce to an acceptable minimum the health risks associated with working in environments with high contents of particulate matter.

1.2 Particulate matter and health effects.

 Particulate matter, suspended in air, forms aerosols. Aerosols are liquid droplets or solid particles of fine enough particle size to remain dispersed in air for a prolonged period (Plog & Quinlan, 2012). The main hazard of particulate matter in aerosols is that it can be inhaled and lodge in the respiratory tract, where it precipitates and can produce toxic reactions.

Particulate matter (PM) can be soluble or insoluble. Soluble PM dissolves on the fluids that cover the respiratory tract, which increases its chances to be absorbed by the body and produce toxic reactions. Insoluble PM, on the other hand, can be expelled by the natural defense mechanisms of the body, or deposit and remain in the lungs, where they may cause chronic lung disease. Particles greater than 100 µm do not get inhaled due to their size; however, particles in the range 0.001 to 100 µm do. As explained earlier, particles of size smaller than 2 µm precipitate in the lungs and cause disease. Figure 1.1 (Plog & Quinlan, 2012) shows the size range of different particulate matter. The range of particles collected for the purpose of the inertial cascade impactor designed in this research is 10 to 0.5 µm. This figure shows that the particulate matter that falls into this range are oil smokes, tobacco smokes, carbon black, metallurgical dust and fume, insecticide dust, viruses and bacteria.

All these types of particulate matter are harmful to human health if a person is exposed to them, in some cases for short periods of times and in other cases for long periods of time. The former case is mainly related to work environments loaded with particulate matter, which could be the case of manufacture plants, or laboratories that handle and study viruses and bacteria. Therefore, it is necessary the use of devices that collect and analyze particulate matter.
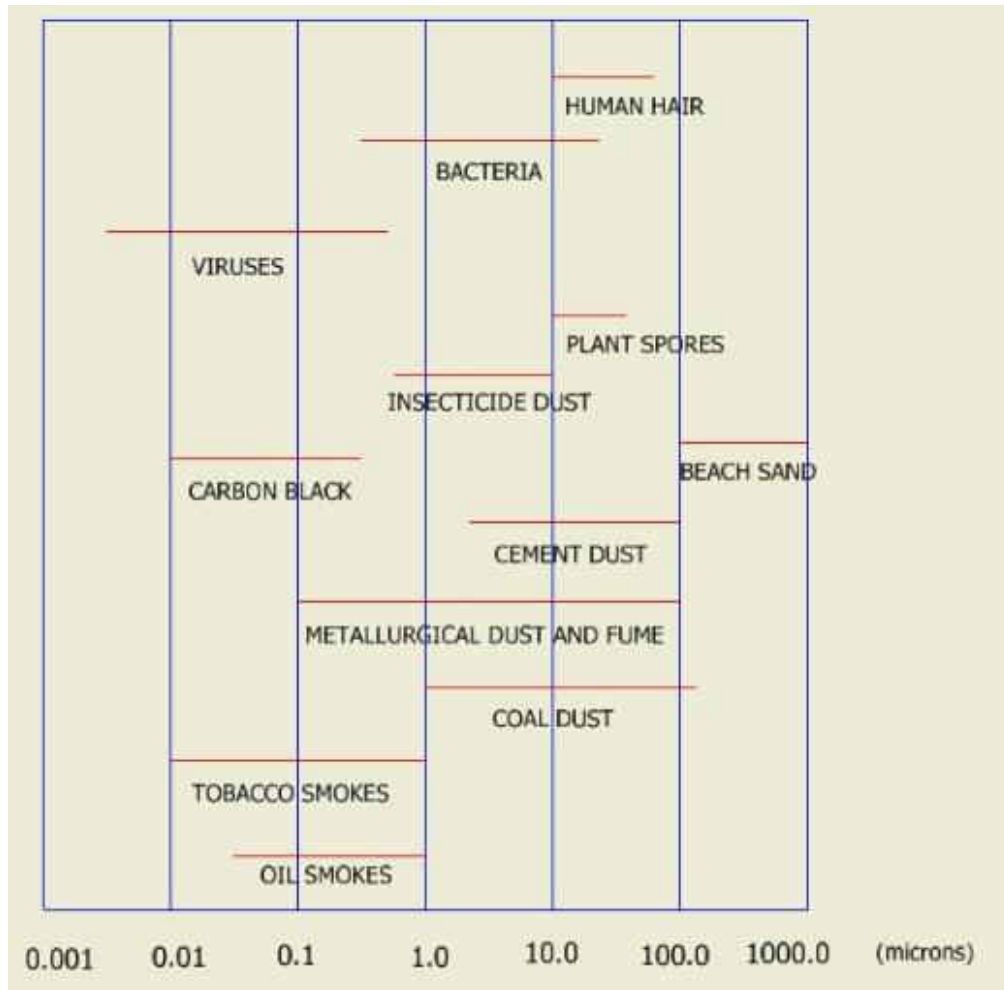
Figure 1.1. Size range of various particulate matter clouds. Source: Plog B. & Quinlan P. (2012).

Particulate matter can be classified in accordance to its composition, size, shape, and how it was created. Table 1.1 (Plog & Quinlan, 2012) shows the general types of particulate matter that can be found in work environments.

Type of PM	Sub-Type	Defining Characteristic	Example/Sources
Dust	General	Produced by mechanical action on larger pieces of the material (e.g., grinding, cutting. tearing)	• Lead dust while scrapping paint • Quartz dust when jack hammering
	Fibers	Dust classified because of its shape as long thin tendrils	• Asbestos • Ceramic fibers • Fiberglass
	Biological (not microorganisms)	Typically, organic dusts created by disturbance of plant or animal materials	• Wood dust • Cotton dust • Animal dander
	Radioactive	Radotoxicity is often more significant than chemical toxicity	• Radon progeny • Radioactive waste • Uranium
Mist	General	Droplets of liquid. Always defined in the context of an aerosol. Created by mechanical action breaking liquid into small particles.	• Droplets from bubbling dip tanks • Paint overspray
	Fog	Droplets of liquid caused by recondensation of vapor	• Boiling acids in chemical digestion
Fume	All	Formed by the evaporation and rapid condensation of metal vapor into vary small particles.	• Welding • Arc or torch cutting • Foundry work
Biological agents	All	These include living and nonliving agents that may be allergenic, toxigenic, or infectious.	• Bacteria (and related organisms) • Viruses • Fungal spores
Smokes	All	Smokes are the products of incomplete combustion of organic materials. Created by vaporization of organic material with subsequent condensation. Sometimes used interchangeably with "fumes".	• Diesel exhaust • Coke -or coal-powered furnaces • Human tissue during laser surgery • Secondhand cigarette smoke

Table 1.1. General Types of Particulate Matter. Source: Plog B. & Quinlan P. (2012).

The myriad of health-related hazards associated exposure to aerosols in work environments, as well as due to air pollution, lead to the need of finding a way to measure the concentration of particulate matter contained within them. Table 1.2 shows a list of some of these health-related effects.

Agent	Typical Industries/Occupations for Exposure	Summary of Health Effects
Arsenic and Inorganic Compounds	Agriculture; wood treatment; semiconductor wafer fabrication (gallium arsenide); alloy production; pesticide manufacture; lead smelting	Inhalation of inorganic arsenic compounds can cause chronic poisoning with weakness, nausea, respiratory tract symptoms, and damage to the peripheral nervous system; cancer
Asbestos	Asbestos abatement; demolition; building maintenance; custodial work; brake repair and replacement	Inhalation increases the risk of lung cancer, mesothelioma (a cancer of the lining of the lungs and peritoneum), asbestosis
Bacteria	Office work; hospitals; sewer repair and maintenance; biological research; social service industries; grade school teaching	Exposure to airborne bacteria may cause indoor air quality problems, humidifier fever, alveolar inflammation or infection
Beryllium and compounds	Aerospace; nuclear industries; electronics; mining and processing; tool manufacturers; refractory ceramic industries; chemical research; sporting goods manufacturing; machining	Chronic exposure to beryllium metal, the oxides, and other insoluble compounds may cause chronic beryllium disease and cancer. Very high exposure to soluble compounds may cause acute beryllium disease
Lead and compounds	Painting; demolition; lead abatement; battery manufacture and maintenance; welding and cutting; brazing; building maintenance; radiation users; machining	One of the most common industrial illnesses is chronic lead poisoning, which manages the peripheral and central nervous systems, sometimes irreversible
Manganese and compounds	Steel manufacturing; alloy making; paint manufacture; chemical research	Inhalation may cause severe damage to the central nervous system, sometimes mimicking Parkinson's disease

Table 1.2. Common particulate matter and their health effects. Source: Plog B. & Quinlan P. (2012).

There are several devices designed for determining the content of particulate matter in aerosols. The focus of this research work is the design of an inertial cascade impactor, which is a common device used to determine the distribution of particles in aerosols by their sizes. Chapter 2 discusses the theoretical basis of these devices.

CHAPTER 2

INERTIAL CASCADE IMPACTORS

2.1 Theoretical study of inertial cascade impactors.

Inertial cascade impactors are instruments that separate the particulate matter in aerosol samples by using the inertia of its particles, which depends on a particle's velocity and aerodynamic size. These devices do not require the knowledge of a particle's density or shape to determine its aerodynamic size . Determining this parameter is important when conducting pharmaceutical and air polluting studies.

Cascade impactors are made of several stages, ranging from 1 to up to 8 in some cases, which can be placed either horizontally, or stacked. Each stage, on stacked cascade impactors, is made up of two plates. One of the plates can contain up to 400 holes drilled in it. These holes can be circular or rectangular, and act as nozzles or jets, through which an aerosol sample is pumped in by an external vacuum pump. The size of these holes is gradually reduced on downstream stages in order to produce higher airstream velocities, which in turn cause smaller particles to deposit on downstream collection plates.

When an aerosol sample passes through an orifice, particles suspended on it move with the same speed as the airstream. As air exits the orifice (also known as nozzle or jet) it is forced to change its direction by 90°, but not all the particles that make up the aerosol can make this turn. Bigger particles, which possess higher inertia, will impact on the collection plate while smaller particles will continue flowing with the airstream. A particle's aerodynamic size, velocity, and density influence its impacting behavior, since a particle's inertia itself depends on these factors. Figure 2.1 shows a schematic of this particle's behavior for spherical-shaped particles of different sizes.
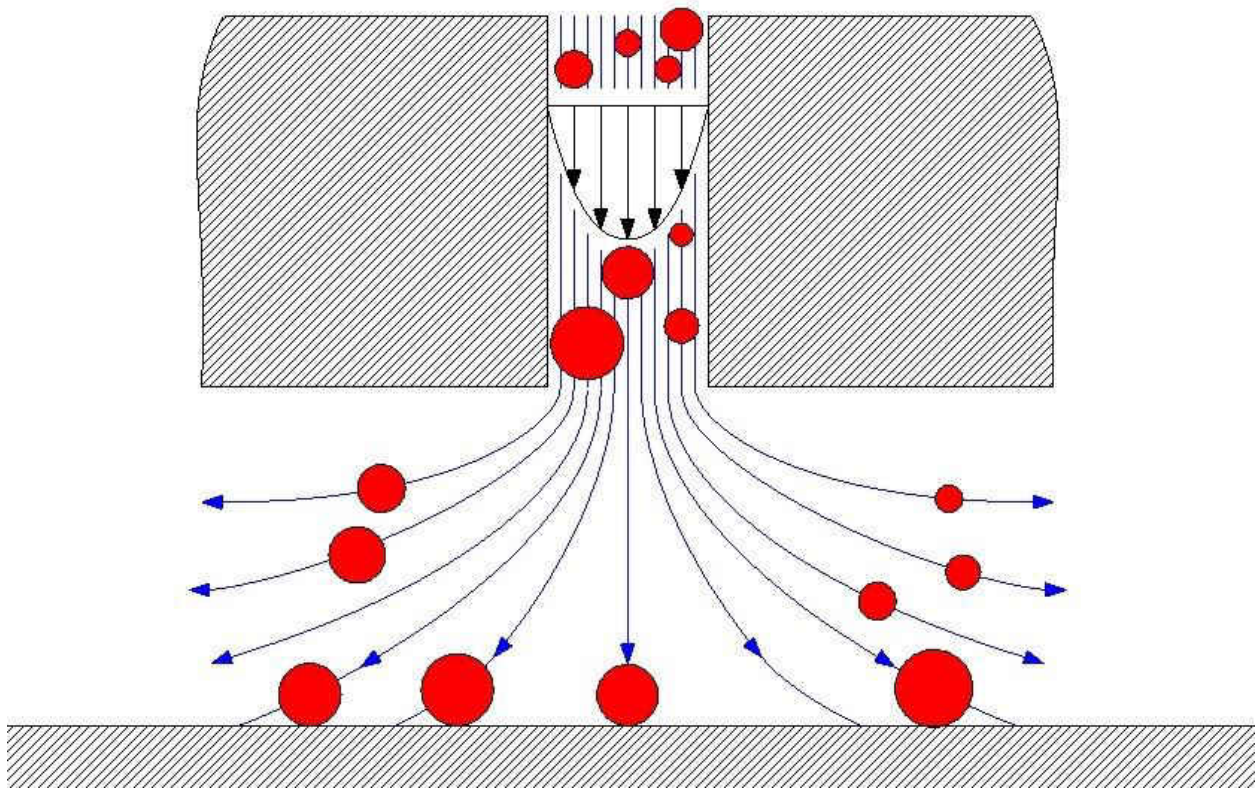
Figure 2.1. Particles impacting on collection plate after passing through nozzle

This process takes place on each nozzle, and eventually particles with higher inertia accumulate on each collection plate; it repeats on each stage which produces particle accumulation on each collection plate according to their sizes. It is important to mention that particles can impact on their respective collection plates, bounce, and return to the airflow, which causes these particles to accumulate on collection plates not meant for their sizes. One way to avoid bouncing is coating the collection plate surface with an oily substance. Glycerin or silicone oil may be used for this purpose.

Aerosol flow through a cascade impactor is highly complex due to the geometric features of this device. The air carrying suspended particles is forced to flow through the internal cavities of the cascade impactor; these cavities include the nozzles of each stage, as well as spaces around the

collection plates. A simple way to describe aerosol flow through a cascade impactor is by dividing it in a Poiseuille flow through each nozzle and then as a stagnation-point flow; however, utilizing only these two types of flow to model the total flow, oversimplifies the real nature of this flow; which could lead to extreme inaccuracies. For instance, this model would neglect the interaction among all the nozzles flow once the aerosol sample exits each nozzle, as well as wall loss and particle bouncing on the collection plates, which are very important factors when designing cascade impactors.

Despite this complexity, the flow in a cascade impactor can be modeled as a two-dimensional axisymmetric flow, which greatly simplifies its analysis; even so, numerical methods are necessary to obtain reasonably accurate results. The next section deals with the theoretical model used for analyzing cascade impactor flow.

2.2 Determination of flow field for round-jet cascade impactor.

Marple (1970) provided a numerical solution to the flow field in one nozzle, for both rectangular and round nozzle shapes. The main idea of his approach was to use the conservation of mass and conservation of momentum in cylindrical coordinates. The Navier-Stokes equations in both the r- and z-direction were utilized, then the momentum equation in the r-direction was differentiated with respect to z, and the z-direction momentum equation was differentiated with respect to r. After this, the resulting equations were subtracted, which eliminated the pressure terms on each equation. Marple (1970) suggested the use of definitions of stream function and vorticity to further simplify the resulting equations, that would lead to obtain a system of two partial differential equations expressed them in terms of nondimensional $\frac{\xi'}{r'}$. A brief discussion of this procedure, for the flow through one round nozzle in one stage, is shown.

The Navier-Stokes equations in cylindrical coordinates were used in this research in order to determine the fluid flow in a stage of the cascade impactor under consideration.

Here, the cylindrical coordinates are represented by (r, θ, z), and the velocity components are represented by (u_r, u_θ, u_z).

The incompressible continuity equation is given by

$$\frac{1}{r}\frac{\partial(ru_r)}{\partial r} + \frac{1}{r}\frac{\partial(u_\theta)}{\partial\theta} + \frac{\partial(u_z)}{\partial z} = 0 \tag{2.1}$$

The equation for the r-component of the incompressible Navier-Stokes Equation is given by

$$\rho\left(\frac{\partial u_r}{\partial t} + u_r\frac{\partial u_r}{\partial r} + \frac{u_\theta}{r}\frac{\partial u_r}{\partial\theta} - \frac{u_\theta^2}{r} + u_z\frac{\partial u_r}{\partial z}\right)$$

$$= -\frac{\partial P}{\partial r} + \rho g_r + \mu\left[\frac{1}{r}\frac{\partial}{\partial r}\left(r\frac{\partial u_r}{\partial r}\right) - \frac{u_r}{r^2} + \frac{1}{r^2}\frac{\partial^2 u_r}{\partial\theta^2} - \frac{2}{r^2}\frac{\partial u_\theta}{\partial\theta} + \frac{\partial^2 u_r}{\partial z^2}\right] \tag{2.2}$$

The equation for the θ-component of the incompressible Navier-Stokes Equation is given by

$$\rho\left(\frac{\partial u_\theta}{\partial t} + u_r\frac{\partial u_\theta}{\partial r} + \frac{u_\theta}{r}\frac{\partial u_\theta}{\partial\theta} + \frac{u_r u_\theta}{r} + u_z\frac{\partial u_\theta}{\partial z}\right)$$

$$= -\frac{1}{r}\frac{\partial P}{\partial\theta} + \rho g_\theta$$

$$+ \mu\left[\frac{1}{r}\frac{\partial}{\partial r}\left(r\frac{\partial u_\theta}{\partial r}\right) - \frac{u_\theta}{r^2} + \frac{1}{r^2}\frac{\partial^2 u_\theta}{\partial\theta^2} + \frac{2}{r^2}\frac{\partial u_r}{\partial\theta} + \frac{\partial^2 u_\theta}{\partial z^2}\right] \tag{2.3}$$

The equation for the z-component of the incompressible Navier-Stokes Equation is given by

$$\rho\left(\frac{\partial u_z}{\partial t} + u_r\frac{\partial u_z}{\partial r} + \frac{u_\theta}{r}\frac{\partial u_z}{\partial\theta} + u_z\frac{\partial u_z}{\partial z}\right)$$

$$= -\frac{\partial P}{\partial z} + \rho g_z + \mu\left[\frac{1}{r}\frac{\partial}{\partial r}\left(r\frac{\partial u_z}{\partial r}\right) + \frac{1}{r^2}\frac{\partial^2 u_z}{\partial\theta^2} + \frac{\partial^2 u_z}{\partial z^2}\right] \tag{2.4}$$

Assumptions

- Diameter of entrance << hole length; therefore, assume fully developed flow (entrance effects negligible)

- Low Reynolds number; therefore, assume laminar flow

- 2-D axisymmetric flow

- Steady State; therefore $\frac{\partial u_r}{\partial t} = \frac{\partial u_\theta}{\partial t} = \frac{\partial u_z}{\partial t} = 0$

- Isothermal; therefore, density and viscosity are constant

- No gravity effects in the radial and angular directions; therefore, $g_r = g_\theta = 0$

- $u_\theta = 0$: The angular component of velocity does not change with respect to the radius of the circular cross-sectional area; therefore, there is no angular component that could cause a change in the angular velocity component.

$$u_r \frac{\partial u_\theta}{\partial r} = \frac{u_\theta}{r}\frac{\partial u_\theta}{\partial \theta} = \frac{u_r u_\theta}{r} = u_z \frac{\partial u_\theta}{\partial z} = 0 \tag{2.5}$$

- The velocity components in the z-direction and the r-direction do not depend on the angle θ due to the axisymmetric flow of the cylindrical hole and stagnation point flow; therefore, we can state that

$$\frac{\partial u_r}{\partial \theta} = \frac{\partial u_z}{\partial \theta} = 0 \tag{2.6}$$

Applying these assumptions to Equation 2.1

$$\frac{1}{r}\frac{\partial(ru_r)}{\partial r} + \frac{1}{r}\frac{\partial(u_\theta)}{\partial \theta} + \frac{\partial(u_z)}{\partial z} = 0 \tag{2.7}$$

$$\frac{1}{r}\frac{\partial(ru_r)}{\partial r} + \frac{\partial(u_z)}{\partial z} = 0 \tag{2.8}$$

but

$$\frac{1}{r}\frac{\partial(ru_r)}{\partial r} = \frac{1}{r}\left(r\frac{\partial u_r}{\partial r} + u_r\right) = \frac{\partial u_r}{\partial r} + \frac{1}{r}u_r \tag{2.9}$$

Therefore

$$\frac{\partial u_r}{\partial r} + \frac{1}{r}u_r + \frac{\partial u_z}{\partial z} = 0 \tag{2.10}$$

Applying these assumptions to Equation 2.2

$$\rho\left(\frac{\partial u_r}{\partial t} + u_r\frac{\partial u_r}{\partial r} + \frac{u_\theta}{r}\frac{\partial u_r}{\partial \theta} - \frac{u_\theta^2}{r} + u_z\frac{\partial u_r}{\partial z}\right)$$

$$= -\frac{\partial P}{\partial r} + \rho g_r + \mu\left[\frac{1}{r}\frac{\partial}{\partial r}\left(r\frac{\partial u_r}{\partial r}\right) - \frac{u_r}{r^2} + \frac{1}{r^2}\frac{\partial^2 u_r}{\partial \theta^2} - \frac{2}{r^2}\frac{\partial u_\theta}{\partial \theta} + \frac{\partial^2 u_r}{\partial z^2}\right] \tag{2.11}$$

$$\rho\left(u_r\frac{\partial u_r}{\partial r} + u_z\frac{\partial u_r}{\partial z}\right) = -\frac{\partial P}{\partial r} + \mu\left[\frac{1}{r}\frac{\partial}{\partial r}\left(r\frac{\partial u_r}{\partial r}\right) - \frac{u_r}{r^2} + \frac{\partial^2 u_r}{\partial z^2}\right] \tag{2.12}$$

But

$$\frac{1}{r}\frac{\partial}{\partial r}\left(r\frac{\partial u_r}{\partial r}\right) = \frac{1}{r}\left[r\frac{\partial}{\partial r}\left(\frac{\partial u_r}{\partial r}\right) + \frac{\partial u_r}{\partial r}\right] = \frac{1}{r}\left(r\frac{\partial^2 u_r}{\partial r^2} + \frac{\partial u_r}{\partial r}\right) = \frac{\partial^2 u_r}{\partial r^2} + \frac{1}{r}\frac{\partial u_r}{\partial r} \qquad (2.13)$$

Therefore

$$\rho\left(u_r\frac{\partial u_r}{\partial r} + u_z\frac{\partial u_r}{\partial z}\right) = -\frac{\partial P}{\partial r} + \mu\left(\frac{\partial^2 u_r}{\partial r^2} + \frac{1}{r}\frac{\partial u_r}{\partial r} - \frac{u_r}{r^2} + \frac{\partial^2 u_r}{\partial z^2}\right) \qquad (2.14)$$

Applying these assumptions to Equation 2.3

$$\rho\left(\frac{\partial u_\theta}{\partial t} + u_r\frac{\partial u_\theta}{\partial r} + \frac{u_\theta}{r}\frac{\partial u_\theta}{\partial \theta} + \frac{u_r u_\theta}{r} + u_z\frac{\partial u_\theta}{\partial z}\right)$$

$$= -\frac{1}{r}\frac{\partial P}{\partial \theta} + \rho g_\theta + \mu\left[\frac{1}{r}\frac{\partial}{\partial r}\left(r\frac{\partial u_\theta}{\partial r}\right) - \frac{u_\theta}{r^2} + \frac{1}{r^2}\frac{\partial^2 u_\theta}{\partial \theta^2} + \frac{2}{r^2}\frac{\partial u_r}{\partial \theta} + \frac{\partial^2 u_\theta}{\partial z^2}\right] \quad (2.15)$$

$$0 = -\frac{1}{\rho}\frac{1}{r}\frac{\partial P}{\partial \theta} \qquad (2.16)$$

$$\frac{\partial P}{\partial \theta} = 0 \qquad (2.17)$$

Recalling that from the continuity Equation we obtained $\frac{\partial u_z}{\partial z} = 0$; therefore $\frac{\partial^2 u_z}{\partial z^2} = 0.$

Applying these assumptions to Equation 2.4 we obtain

$$\rho\left(\frac{\partial u_z}{\partial t} + u_r\frac{\partial u_z}{\partial r} + \frac{u_\theta}{r}\frac{\partial u_z}{\partial \theta} + u_z\frac{\partial u_z}{\partial z}\right)$$

$$= -\frac{\partial P}{\partial z} + \rho g_z + \mu\left[\frac{1}{r}\frac{\partial}{\partial r}\left(r\frac{\partial u_z}{\partial r}\right) + \frac{1}{r^2}\frac{\partial^2 u_z}{\partial \theta^2} + \frac{\partial^2 u_z}{\partial z^2}\right] \qquad (2.18)$$

$$\rho\left(u_r\frac{\partial u_z}{\partial r}+u_z\frac{\partial u_z}{\partial z}\right)=-\frac{\partial P}{\partial z}+\rho g_z+\mu\left[\frac{1}{r}\frac{\partial}{\partial r}\left(r\frac{\partial u_z}{\partial r}\right)+\frac{\partial^2 u_z}{\partial z^2}\right] \qquad (2.19)$$

but

$$\frac{1}{r}\frac{\partial}{\partial r}\left(r\frac{\partial u_z}{\partial r}\right)=\frac{1}{r}\left(r\frac{\partial^2 u_z}{\partial r^2}+\frac{\partial u_z}{\partial r}\right)=\frac{\partial^2 u_z}{\partial r^2}+\frac{1}{r}\frac{\partial u_z}{\partial r} \qquad (2.20)$$

$$\rho\left(u_r\frac{\partial u_z}{\partial r}+u_z\frac{\partial u_z}{\partial z}\right)=-\frac{\partial P}{\partial z}+\rho g_z+\mu\left(\frac{\partial^2 u_z}{\partial r^2}+\frac{1}{r}\frac{\partial u_z}{\partial r}+\frac{\partial^2 u_z}{\partial z^2}\right) \qquad (2.21)$$

In addition to Equations 2.10, 2.14, and 2.21, the definitions of stream function and vorticity can be used to model the flow of aerosol through the nozzle and impinging on the collection plate. The stream function in cylindrical coordinates for incompressible and axisymmetric flow is defined as:

$$u_r=\frac{1}{r}\frac{\partial \psi}{\partial z} \qquad (2.22)$$

$$u_z=-\frac{1}{r}\frac{\partial \psi}{\partial r} \qquad (2.23)$$

Çengel & Cimbala (2006) define vorticity in cylindrical coordinates as

$$\vec{\zeta}=\left(\frac{1}{r}\frac{\partial u_z}{\partial \theta}-\frac{\partial u_\theta}{\partial z}\right)\vec{e}_r+\left(\frac{\partial u_r}{\partial z}-\frac{\partial u_z}{\partial r}\right)\vec{e}_\theta+\frac{1}{r}\left[\frac{\partial (ru_\theta)}{\partial r}-\frac{\partial u_r}{\partial \theta}\right]\vec{e}_z \qquad (2.24)$$

But since the flow in through the jet is being modeled as an axisymmetric flow, it was already

stated that $\frac{\partial u_r}{\partial \theta} = \frac{\partial u_z}{\partial \theta} = \frac{\partial u_\theta}{\partial z} = \frac{\partial (r u_\theta)}{\partial r} = 0$; therefore equation 2.24 becomes

$$\vec{\zeta} = \left(\frac{\partial u_z}{\partial r} - \frac{\partial u_r}{\partial z} \right) \vec{e}_\theta \tag{2.25}$$

Marple (1970) solved the system of equations 2.10, 2.14, 2.21, 2.22, 2.23, and 2.25 by

nondimensionalizing them using the following dimensionless terms:

$$r' = \frac{r}{W} \tag{2.26}$$

$$\psi' = \frac{\psi}{U_0 W^2} \tag{2.27}$$

$$\frac{\zeta'}{r'} = \frac{\frac{\zeta}{r}}{\frac{U_0}{W^2}} = \frac{\zeta W^2}{r U_0} \tag{2.28}$$

$$z' = \frac{z}{W} \tag{2.29}$$

$$Re = \frac{\rho U_0 W}{\mu} \tag{2.30}$$

Table 2.1 summarizes the equations that make up the system that is used to model the flow in

one stage of an inertial cascade impactor.

Equation	Number
$$\frac{\partial u_r}{\partial r} + \frac{1}{r}u_r + \frac{\partial u_z}{\partial z} = 0$$	2.10
$$\rho\left(u_r\frac{\partial u_r}{\partial r} + u_z\frac{\partial u_r}{\partial z}\right) = -\frac{\partial P}{\partial r} + \mu\left(\frac{\partial^2 u_r}{\partial r^2} + \frac{1}{r}\frac{\partial u_r}{\partial r} - \frac{u_r}{r^2} + \frac{\partial^2 u_r}{\partial z^2}\right)$$	2.14
$$\rho\left(u_r\frac{\partial u_z}{\partial r} + u_z\frac{\partial u_z}{\partial z}\right) = -\frac{\partial P}{\partial z} + \rho g_z + \mu\left(\frac{\partial^2 u_z}{\partial r^2} + \frac{1}{r}\frac{\partial u_z}{\partial r} + \frac{\partial^2 u_z}{\partial z^2}\right)$$	2.21
$$u_r = \frac{1}{r}\frac{\partial \psi}{\partial z}$$	2.22
$$u_z = -\frac{1}{r}\frac{\partial \psi}{\partial r}$$	2.23
$$\vec{\zeta} = \left(\frac{\partial u_z}{\partial r} - \frac{\partial u_r}{\partial z}\right)\vec{e}_\theta$$	2.25

Table 2.1. Governing equations for fluid flow in one stage

Dividing Equation 2.4 by ρ, and since $\nu = \frac{\mu}{\rho}$

$$u_r\frac{\partial u_r}{\partial r} + u_z\frac{\partial u_r}{\partial z} = -\frac{1}{\rho}\frac{\partial P}{\partial r} + \nu\left(\frac{\partial^2 u_r}{\partial r^2} + \frac{1}{r}\frac{\partial u_r}{\partial r} - \frac{u_r}{r^2} + \frac{\partial^2 u_r}{\partial z^2}\right) \tag{2.31}$$

Differentiating Equation 2.31 with respect to z

$$\frac{\partial}{\partial z}\left(u_r\frac{\partial u_r}{\partial r}\right) + \frac{\partial}{\partial z}\left(u_z\frac{\partial u_r}{\partial z}\right)$$

$$= -\frac{1}{\rho}\frac{\partial}{\partial z}\left(\frac{\partial P}{\partial r}\right)$$

$$+ \nu\left[\frac{\partial}{\partial z}\left(\frac{\partial^2 u_r}{\partial r^2}\right) + \frac{\partial}{\partial z}\left(\frac{1}{r}\frac{\partial u_r}{\partial r}\right) - \frac{\partial}{\partial z}\left(\frac{u_r}{r^2}\right) + \frac{\partial}{\partial z}\left(\frac{\partial^2 u_r}{\partial z^2}\right)\right] \tag{2.32}$$

Solving term by term

$$(2.33)$$

$$\frac{\partial}{\partial z}\left(u_r \frac{\partial u_r}{\partial r}\right) = u_r \frac{\partial}{\partial z}\left(\frac{\partial u_r}{\partial r}\right) + \frac{\partial u_r}{\partial r}\frac{\partial u_r}{\partial z} = u_r \frac{\partial^2 u_r}{\partial z \partial r} + \frac{\partial u_r}{\partial r}\frac{\partial u_r}{\partial z} \tag{2.34}$$

$$\frac{\partial}{\partial z}\left(u_z \frac{\partial u_r}{\partial z}\right) = u_z \frac{\partial}{\partial z}\left(\frac{\partial u_r}{\partial z}\right) + \frac{\partial u_r}{\partial z}\frac{\partial u_z}{\partial z} = u_z \frac{\partial^2 u_r}{\partial z^2} + \frac{\partial u_r}{\partial z}\frac{\partial u_z}{\partial z} \tag{2.35}$$

$$-\frac{1}{\rho}\frac{\partial}{\partial z}\left(\frac{\partial P}{\partial r}\right) = -\frac{1}{\rho}\frac{\partial^2 P}{\partial z \partial r} \tag{2.36}$$

$$\frac{\partial}{\partial z}\left(\frac{\partial^2 u_r}{\partial r^2}\right) = \frac{\partial^3 u_r}{\partial z \partial r^2} \tag{2.37}$$

$$\frac{\partial}{\partial z}\left(\frac{1}{r}\frac{\partial u_r}{\partial r}\right) = \frac{1}{r}\frac{\partial}{\partial z}\left(\frac{\partial u_r}{\partial r}\right) + \frac{\partial u_r}{\partial r}\frac{\partial}{\partial z}\left(\frac{1}{r}\right) = \frac{1}{r}\frac{\partial^2 u_r}{\partial z \partial r} + \frac{\partial u_r}{\partial r}(0) = \frac{1}{r}\frac{\partial^2 u_r}{\partial z \partial r} \tag{2.38}$$

$$\frac{\partial}{\partial z}\left(\frac{u_r}{r^2}\right) = \frac{\partial}{\partial z}\left(\frac{1}{r^2}u_r\right) = \frac{1}{r^2}\frac{\partial u_r}{\partial z} + u_r \frac{\partial}{\partial z}\left(\frac{1}{r^2}\right) = \frac{1}{r^2}\frac{\partial u_r}{\partial z} + u_r(0)$$

$$= \frac{1}{r^2}\frac{\partial u_r}{\partial z} \tag{2.39}$$

$$\frac{\partial}{\partial z}\left(\frac{\partial^2 u_r}{\partial z^2}\right) = \frac{\partial^3 u_r}{\partial z^3} \tag{2.40}$$

Substituting in Equation 2.31

$$u_r \frac{\partial^2 u_r}{\partial z \partial r} + \frac{\partial u_r}{\partial r}\frac{\partial u_r}{\partial z} + u_z \frac{\partial^2 u_r}{\partial z^2} + \frac{\partial u_r}{\partial z}\frac{\partial u_z}{\partial z}$$

$$= -\frac{1}{\rho}\frac{\partial^2 P}{\partial z \partial r} + \nu\left(\frac{\partial^3 u_r}{\partial z \partial r^2} + \frac{1}{r}\frac{\partial^2 u_r}{\partial z \partial r} - \frac{1}{r^2}\frac{\partial u_r}{\partial z} + \frac{\partial^3 u_r}{\partial z^3}\right) \tag{2.41}$$

Dividing Equation 2.21 by ρ, and since $v = \frac{\mu}{\rho}$

$$u_r \frac{\partial u_z}{\partial r} + u_z \frac{\partial u_z}{\partial z} = -\frac{1}{\rho} \frac{\partial P}{\partial z} + g_z + v \left(\frac{\partial^2 u_z}{\partial r^2} + \frac{1}{r} \frac{\partial u_z}{\partial r} + \frac{\partial^2 u_z}{\partial z^2} \right) \tag{2.42}$$

Differentiating Equation 2.41 with respect to r

$$\frac{\partial}{\partial r} \left(u_r \frac{\partial u_z}{\partial r} \right) + \frac{\partial}{\partial r} \left(u_z \frac{\partial u_z}{\partial z} \right)$$

$$= -\frac{\partial}{\partial r} \left(\frac{1}{\rho} \frac{\partial P}{\partial z} \right) + \frac{\partial g_z}{\partial r}$$

$$+ v \left[\frac{\partial}{\partial r} \left(\frac{\partial^2 u_z}{\partial r^2} \right) + \frac{\partial}{\partial r} \left(\frac{1}{r} \frac{\partial u_z}{\partial r} \right) + \frac{\partial}{\partial r} \left(\frac{\partial^2 u_z}{\partial z^2} \right) \right] \tag{2.43}$$

Solving term by term

$$\frac{\partial}{\partial r} \left(u_r \frac{\partial u_z}{\partial r} \right) = u_r \frac{\partial}{\partial r} \left(\frac{\partial u_z}{\partial r} \right) + \frac{\partial u_z}{\partial r} \frac{\partial u_r}{\partial r} = u_r \frac{\partial^2 u_z}{\partial r^2} + \frac{\partial u_z}{\partial r} \frac{\partial u_r}{\partial r} \tag{2.44}$$

$$\frac{\partial}{\partial r} \left(u_z \frac{\partial u_z}{\partial z} \right) = u_z \frac{\partial}{\partial r} \left(\frac{\partial u_z}{\partial z} \right) + \frac{\partial u_z}{\partial z} \frac{\partial u_z}{\partial r} = u_z \frac{\partial^2 u_z}{\partial r \partial z} + \frac{\partial u_z}{\partial z} \frac{\partial u_z}{\partial r} \tag{2.45}$$

$$-\frac{\partial}{\partial r} \left(\frac{1}{\rho} \frac{\partial P}{\partial z} \right) = -\frac{1}{\rho} \frac{\partial}{\partial r} \left(\frac{\partial P}{\partial z} \right) = -\frac{1}{\rho} \frac{\partial^2 P}{\partial r \partial z} \tag{2.46}$$

$$\frac{\partial g_z}{\partial r} = 0 \tag{2.47}$$

$$\frac{\partial}{\partial r} \left(\frac{\partial^2 u_z}{\partial r^2} \right) = \frac{\partial^3 u_z}{\partial r^3} \tag{2.48}$$

$$\frac{\partial}{\partial r} \left(\frac{1}{r} \frac{\partial u_z}{\partial r} \right) = \frac{1}{r} \frac{\partial}{\partial r} \left(\frac{\partial u_z}{\partial r} \right) + \frac{\partial u_z}{\partial r} \frac{\partial}{\partial r} \left(\frac{1}{r} \right) = \frac{1}{r} \frac{\partial^2 u_z}{\partial r^2} - \frac{1}{r^2} \frac{\partial u_z}{\partial r} \tag{2.49}$$

$$\frac{\partial}{\partial r}\left(\frac{\partial^2 u_z}{\partial z^2}\right) = \frac{\partial^3 u_z}{\partial r \partial z^2} \tag{2.50}$$

Substituting in Equation 2.41

$$u_r \frac{\partial^2 u_z}{\partial r^2} + \frac{\partial u_z}{\partial r}\frac{\partial u_r}{\partial r} + u_z \frac{\partial^2 u_z}{\partial r \partial z} + \frac{\partial u_z}{\partial z}\frac{\partial u_z}{\partial r}$$

$$= -\frac{1}{\rho}\frac{\partial^2 P}{\partial r \partial z} + v\left(\frac{\partial^3 u_z}{\partial r^3} + \frac{1}{r}\frac{\partial^2 u_z}{\partial r^2} - \frac{1}{r^2}\frac{\partial u_z}{\partial r} + \frac{\partial^3 u_z}{\partial r \partial z^2}\right) \tag{2.51}$$

Comparing Equations 2.41 and 2.51, we can notice that the pressure term is made up of mixed partial derivatives; if P represents a continuous function, we can use Clairaut's Theorem, and state that

$$-\frac{1}{\rho}\frac{\partial^2 P}{\partial z \partial r} = -\frac{1}{\rho}\frac{\partial^2 P}{\partial r \partial z} \tag{2.52}$$

Now, subtracting Equation 2.16 from Equation 2.14

$$u_r \frac{\partial^2 u_r}{\partial z \partial r} + \frac{\partial u_r}{\partial r}\frac{\partial u_r}{\partial z} + u_z \frac{\partial^2 u_r}{\partial z^2} + \frac{\partial u_r}{\partial z}\frac{\partial u_z}{\partial z} - u_r \frac{\partial^2 u_z}{\partial r^2} - \frac{\partial u_z}{\partial r}\frac{\partial u_r}{\partial r} - u_z \frac{\partial^2 u_z}{\partial r \partial z} - \frac{\partial u_z}{\partial z}\frac{\partial u_z}{\partial r}$$

$$= -\frac{1}{\rho}\frac{\partial^2 P}{\partial z \partial r} + \frac{1}{\rho}\frac{\partial^2 P}{\partial r \partial z} + v\left(\frac{\partial^3 u_r}{\partial z \partial r^2} + \frac{1}{r}\frac{\partial^2 u_r}{\partial z \partial r} - \frac{1}{r^2}\frac{\partial u_r}{\partial z} + \frac{\partial^3 u_r}{\partial z^3}\right)$$

$$- v\left(\frac{\partial^3 u_z}{\partial r^3} + \frac{1}{r}\frac{\partial^2 u_z}{\partial r^2} - \frac{1}{r^2}\frac{\partial u_z}{\partial r} + \frac{\partial^3 u_z}{\partial r \partial z^2}\right) \tag{2.53}$$

This action will cancel out the pressure terms:

$$u_r \left(\frac{\partial^2 u_r}{\partial z \partial r} - \frac{\partial^2 u_z}{\partial r^2} \right) + u_z \left(\frac{\partial^2 u_r}{\partial z^2} - \frac{\partial^2 u_z}{\partial r \partial z} \right) + \left(\frac{\partial u_r}{\partial z} - \frac{\partial u_z}{\partial r} \right) \left(\frac{\partial u_r}{\partial r} + \frac{\partial u_z}{\partial z} \right)$$

$$= \nu \left(\frac{\partial^3 u_r}{\partial z \partial r^2} + \frac{1}{r} \frac{\partial^2 u_r}{\partial z \partial r} - \frac{1}{r^2} \frac{\partial u_r}{\partial z} + \frac{\partial^3 u_r}{\partial z^3} - \frac{\partial^3 u_z}{\partial r^3} - \frac{1}{r} \frac{\partial^2 u_z}{\partial r^2} \right.$$

$$\left. + \frac{1}{r^2} \frac{\partial u_z}{\partial r} - \frac{\partial^3 u_z}{\partial r \partial z^2} \right) \tag{2.54}$$

From Equation 2.42 (the continuity equation)

$$\frac{\partial u_r}{\partial r} + \frac{1}{r} u_r + \frac{\partial u_z}{\partial z} = 0 \quad \rightarrow$$

$$\frac{\partial u_z}{\partial z} + \frac{\partial u_r}{\partial r} = -\frac{1}{r} u_r \tag{2.55}$$

Substituting Equation 2.55 in Equation 2.54

$$u_r \left(\frac{\partial^2 u_r}{\partial z \partial r} - \frac{\partial^2 u_z}{\partial r^2} \right) + u_z \left(\frac{\partial^2 u_r}{\partial z^2} - \frac{\partial^2 u_z}{\partial r \partial z} \right) - \frac{1}{r} u_r \left(\frac{\partial u_r}{\partial z} - \frac{\partial u_z}{\partial r} \right)$$

$$= \nu \left(\frac{\partial^3 u_r}{\partial z \partial r^2} + \frac{1}{r} \frac{\partial^2 u_r}{\partial z \partial r} - \frac{1}{r^2} \frac{\partial u_r}{\partial z} + \frac{\partial^3 u_r}{\partial z^3} - \frac{\partial^3 u_z}{\partial r^3} - \frac{1}{r} \frac{\partial^2 u_z}{\partial r^2} + \frac{1}{r^2} \frac{\partial u_z}{\partial r} \right.$$

$$\left. - \frac{\partial^3 u_z}{\partial r \partial z^2} \right) \tag{2.56}$$

$$u_r \left(\frac{\partial^2 u_r}{\partial z \partial r} - \frac{\partial^2 u_z}{\partial r^2} - \frac{1}{r} \frac{\partial u_r}{\partial z} + \frac{1}{r} \frac{\partial u_z}{\partial r} \right) + u_z \left(\frac{\partial^2 u_r}{\partial z^2} - \frac{\partial^2 u_z}{\partial r \partial z} \right)$$

$$= \nu \left[\frac{\partial^3 u_r}{\partial z \partial r^2} + \frac{1}{r} \left(\frac{\partial^2 u_r}{\partial z \partial r} - \frac{\partial^2 u_z}{\partial r^2} \right) + \frac{1}{r^2} \left(\frac{\partial u_z}{\partial r} - \frac{\partial u_r}{\partial z} \right) + \frac{\partial^3 u_r}{\partial z^3} \right.$$

$$\left. - \frac{\partial^3 u_z}{\partial r^3} - \frac{\partial^3 u_z}{\partial r \partial z^2} \right] \tag{2.57}$$

Using the definition of stream function in Equation 2.57

$$u_r = \frac{1}{r}\frac{\partial \psi}{\partial z} \tag{2.58}$$

$$u_z = -\frac{1}{r}\frac{\partial \psi}{\partial r} \tag{2.59}$$

Expressing vorticity in terms of the stream function as defined by Marple (1970).

$$\vec{\zeta} = \frac{\partial u_z}{\partial r} - \frac{\partial u_r}{\partial z} \tag{2.60}$$

$$u_r = \frac{1}{r}\frac{\partial \psi}{\partial z} \tag{2.61}$$

$$u_z = -\frac{1}{r}\frac{\partial \psi}{\partial r} \tag{2.62}$$

$$\zeta = \frac{\partial u_z}{\partial r} - \frac{\partial u_r}{\partial z} = -\frac{\partial}{\partial r}\left(\frac{1}{r}\frac{\partial \psi}{\partial r}\right) - \frac{\partial}{\partial z}\left(\frac{1}{r}\frac{\partial \psi}{\partial z}\right) \tag{2.63}$$

After applying these relations to Equations 2.55 and 2.57, some algebraic manipulations, and nondimensionalizing, it is possible to obtain the equations applicable to one stage nozzle in an inertial cascade impactor Marple (1970).

$$r^2 \frac{\partial \left(\frac{\omega}{r}\frac{\partial \psi}{\partial z}\right)}{\partial r} - r^2 \frac{\partial \left(\frac{\omega}{r}\frac{\partial \psi}{\partial r}\right)}{\partial z} = \frac{1}{Re}\left\{\frac{\partial}{\partial r}\left[r^3 \frac{\partial}{\partial r}\left(\frac{\omega}{r}\right)\right] + \frac{\partial}{\partial z}\left[r^3 \frac{\partial}{\partial z}\left(\frac{\omega}{r}\right)\right]\right\} \tag{2.64}$$

$$\frac{\omega}{r}\cdot r = -\frac{\partial}{\partial r}\left(\frac{1}{r}\frac{\partial \psi}{\partial r}\right) - \frac{\partial}{\partial z}\left(\frac{1}{r}\frac{\partial \psi}{\partial z}\right) \tag{2.65}$$

Equations 2.64 and 2.65 can be solved by using the right boundary conditions. Figure 2.2 shows a basic schematic of the flow through a round nozzle. The stream function on Walls 1, 2, and 3 is

constant. Marple (1970) decided to give them the value of zero; besides, he determined that these values are maximum for the centerline of the round nozzles, as well as on Wall 4. On the other hand, along all walls the velocity components are zero.
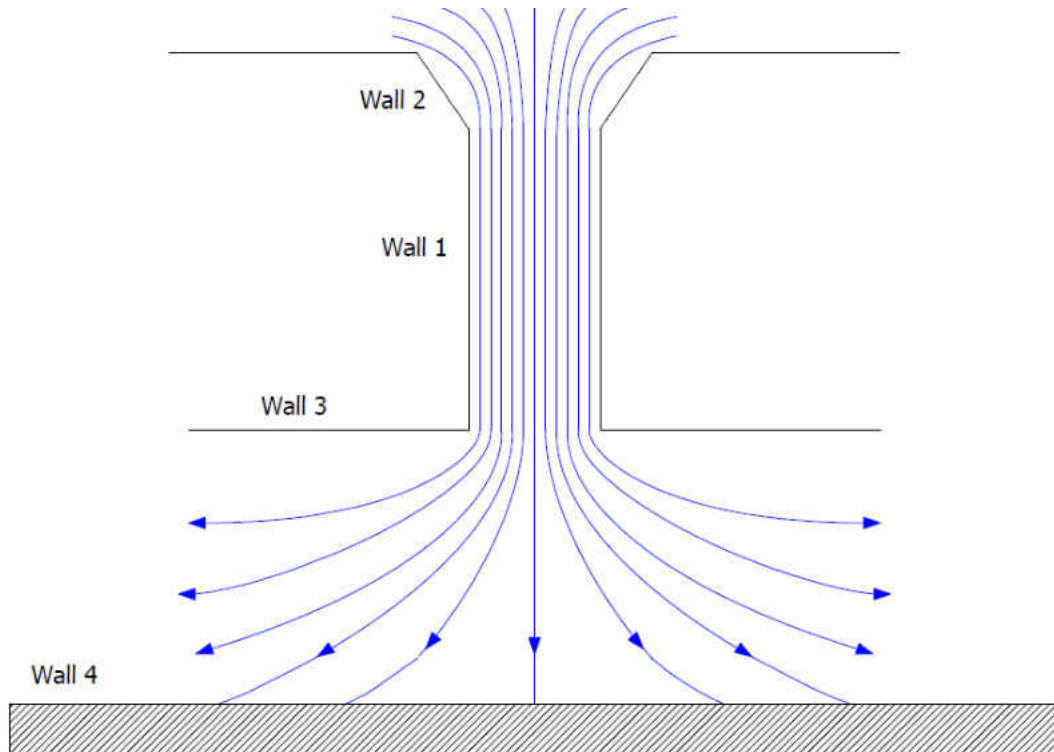

Figure 2.2. Boundary Conditions of the flow through a round nozzle

Marple (1970) solved the system of equations made up by equations 2.64 and 2.65, along with these boundary conditions using a finite difference numerical method. The objective of this thesis was not to solve this system again, but to use COMSOL to model the fluid flow within the inertial cascade impactor, which due to its obvious complexity would not be easily solved using a mathematical or numerical approach.

2.3 Flow simulation using COMSOL.

Before developing the flow simulation in COMSOL, it is necessary to perform initial calculation

of the parameters to be used. It is important to mention that laminar flow was assumed in

modeling the flow through the nozzles.

The flow rate of the pump used in this simulation has can provide an air flow rate of 1.5CFM;

transforming this value to $\frac{m^3}{s}$. The geometric data was taken from the dimensions shown in the

blueprints shown later. All calculations will express the results in the MKS system.

Inlet

$$\dot{Q} = 1.5 \frac{ft^3}{min} \cdot \frac{1\ min}{60\ s} \cdot \frac{1\ m^3}{(3.281\ ft)^3} = 7.08 \cdot 10^{-4} \frac{m^3}{s}$$

$$A_{inlet} = \frac{\pi}{4} D^2 = \frac{\pi}{4} \left(1.250\ in\ \frac{2.54\ cm}{1\ in} \cdot \frac{1\ m}{100\ cm} \right)^2 = 7.92 \cdot 10^{-4}\ m^2$$

$$\dot{Q} = A_{inlet} V_{inlet} \rightarrow V_{inlet} = \frac{\dot{Q}}{A_{inlet}} = \frac{7.08 \cdot 10^{-4} \frac{m^3}{s}}{7.92 \cdot 10^{-4}\ m^2} = 0.894\ \frac{m}{s}.$$

Outlet

$$A_{outlet} = \frac{\pi}{4} D^2 = \frac{\pi}{4} \left(0.375\ in\ \frac{2.54\ cm}{1\ in} \cdot \frac{1\ m}{100\ cm} \right)^2 = 7.1 \cdot 10^{-5}\ m^2$$

$$\dot{Q} = A_{outlet} V_{outlet} \rightarrow V_{outlet} = \frac{\dot{Q}}{A_{outlet}} = \frac{7.08 \cdot 10^{-4} \frac{m^3}{s}}{7.1 \cdot 10^{-5}\ m^2} = 9.972\ \frac{m}{s}.$$

In order to obtain the most accurate results when running COMSOL, it was necessary to use a

kinetic-epsilon turbulent model approach when solving for the velocity field, since at first, a

laminar approach did not produce any convergent solution. Besides, a stationary study was used, since the steady state is what matters most for our purposes.

Figure 2.3 shows the 2D representation of the cavity within the cascade impactor, which is always filled with air.

Figures 2.4 – 2.8 show a detail of the mesh generated by COMSOL at each stage of the cascade impactor. It is important to mention that initially a coarser mesh was utilized to perform the simulation; however, COMSOL was having issues meshing he region around boundary layers, so a finer mesh was utilized to solve this inconvenient.
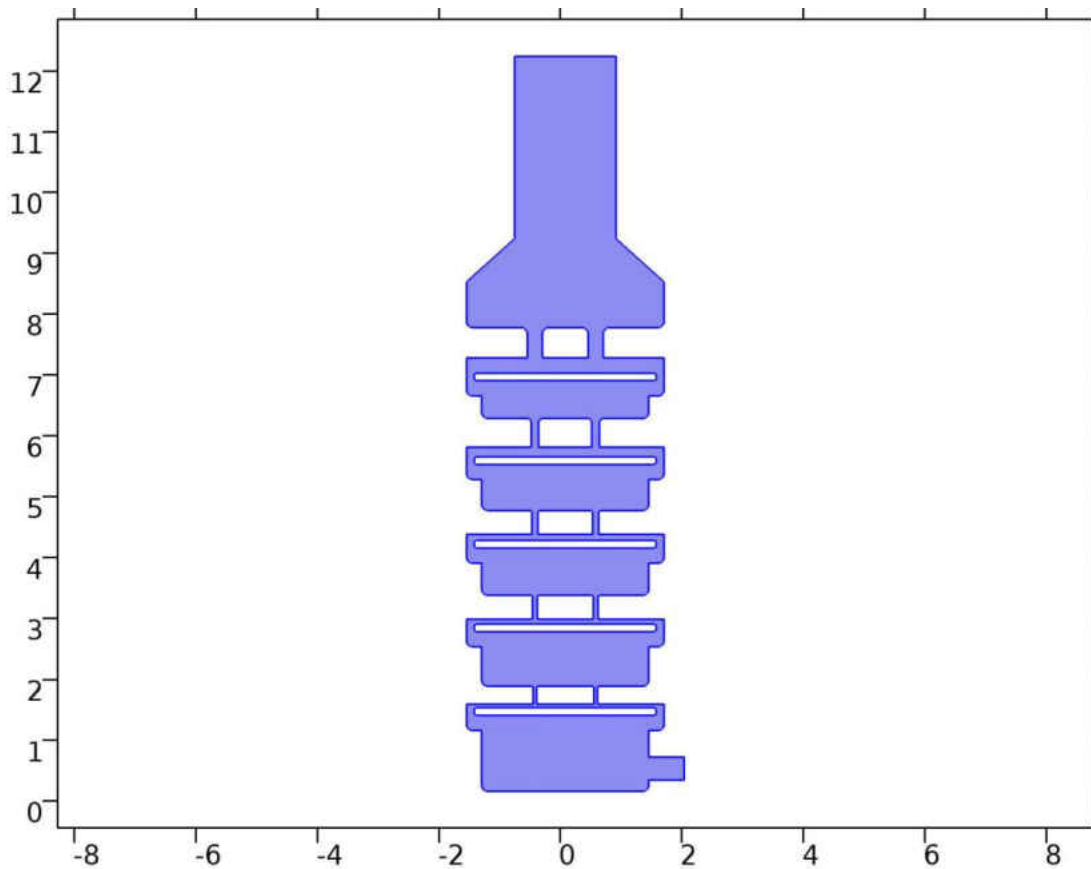

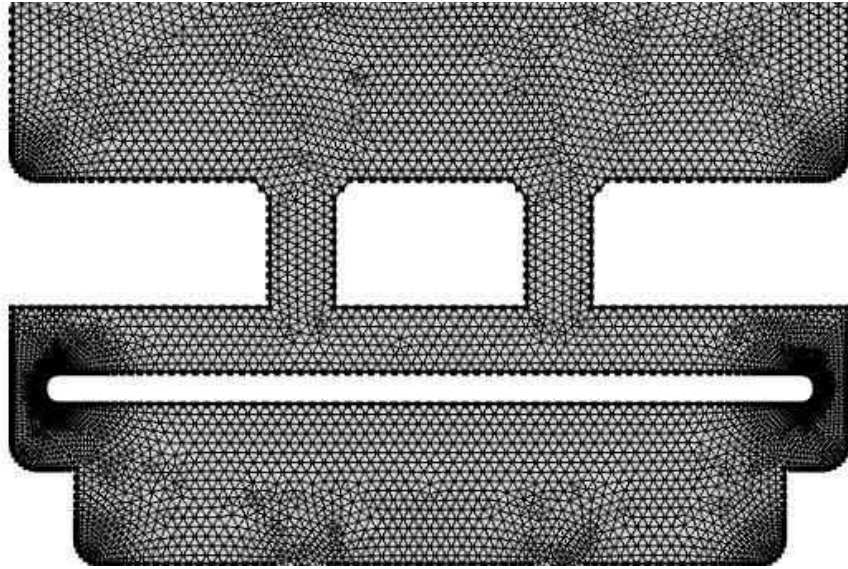Figure 2.3. Internal volume of cascade impactor

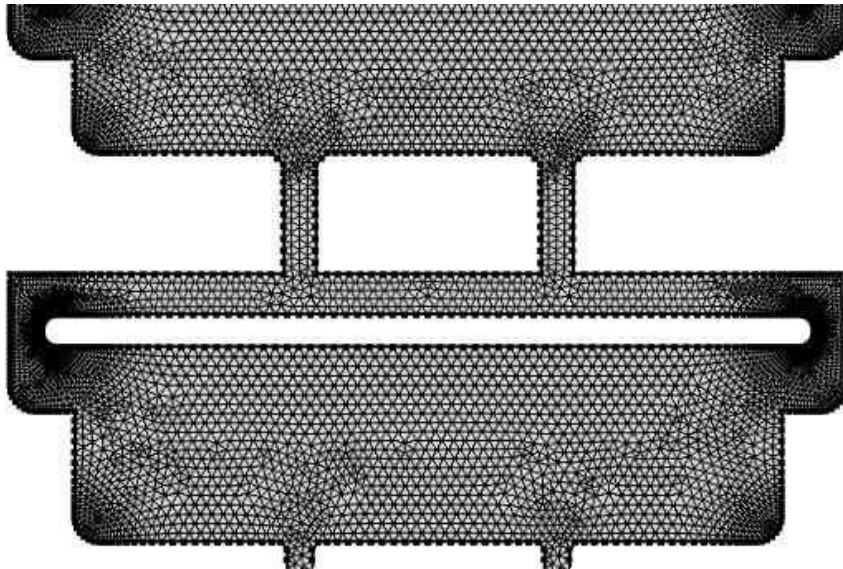Figure 2.4. Stage 1 Mesh generated by COMSOL.

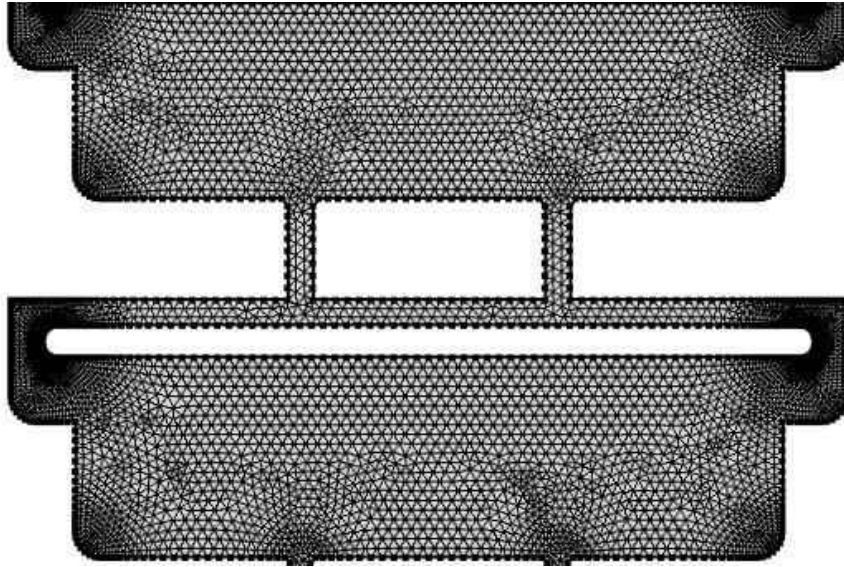Figure 2.5. Stage 2 Mesh generated by COMSOL.
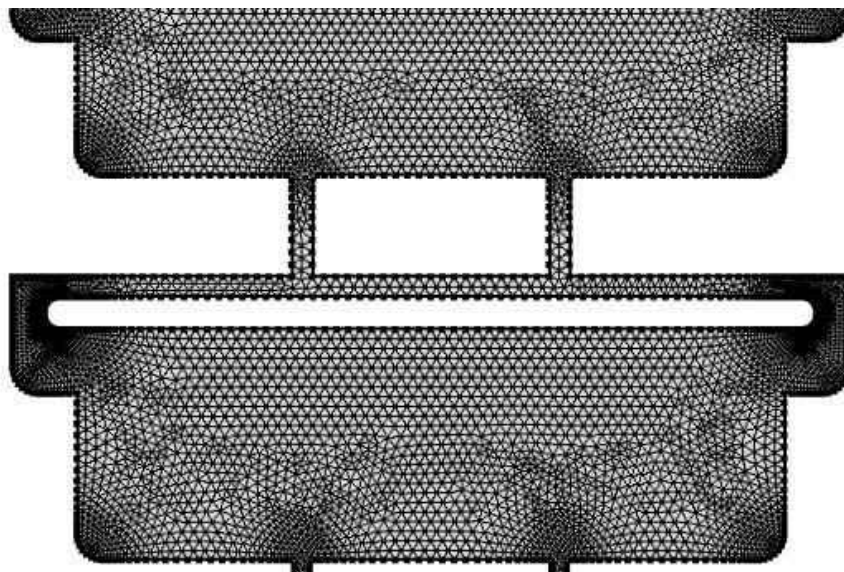
Figure 2.6. Stage 3 Mesh generated by COMSOL.

Figure 2.7. Stage 4 Mesh generated by COMSOL.

Figure 2.8. Stage 5 Mesh generated by COMSOL.

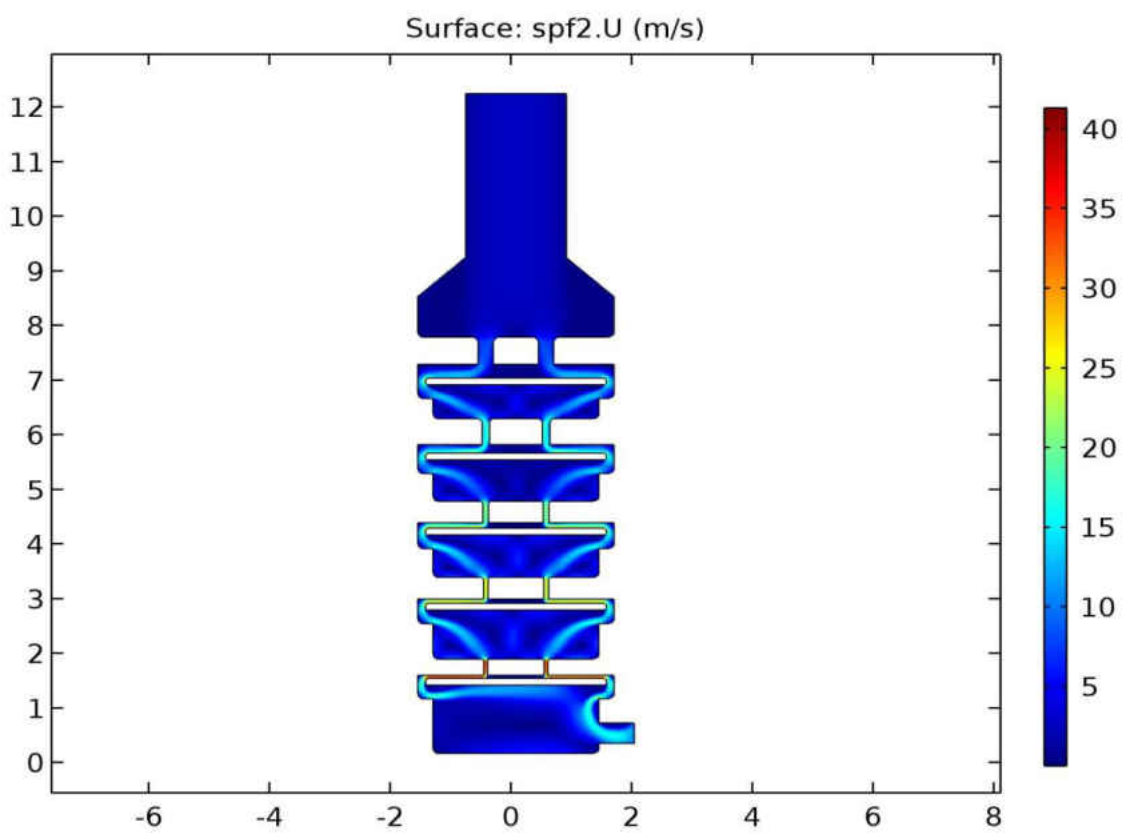After performing the computation, COMSOL yielded a velocity field plot, shown in Figure 2.9.

Figure 2.9. Velocity Field generated by COMSOL.

An important observation from Figure 2.9 is that velocity values away from the collection plate-air interface are lower; the same applies to the regions away from the nozzles. This means that the cascade impactor design can be improved by reducing the height of each stage, which reduces the material needed, therefore making it cheaper to manufacture.

Additionally, Figure 2.9 shows the importance of radii on the inside geometry of the cascade impactor. Nonrounded edges produce sharp changes in the air flow, which are not desirable.

Figure 2.10 shows the pressure field for the cascade impactor cavity. It is observed that pressure decreases from 101.325 kPa (atmospheric), to about 97.0 kPa at the suction port, which is expected.
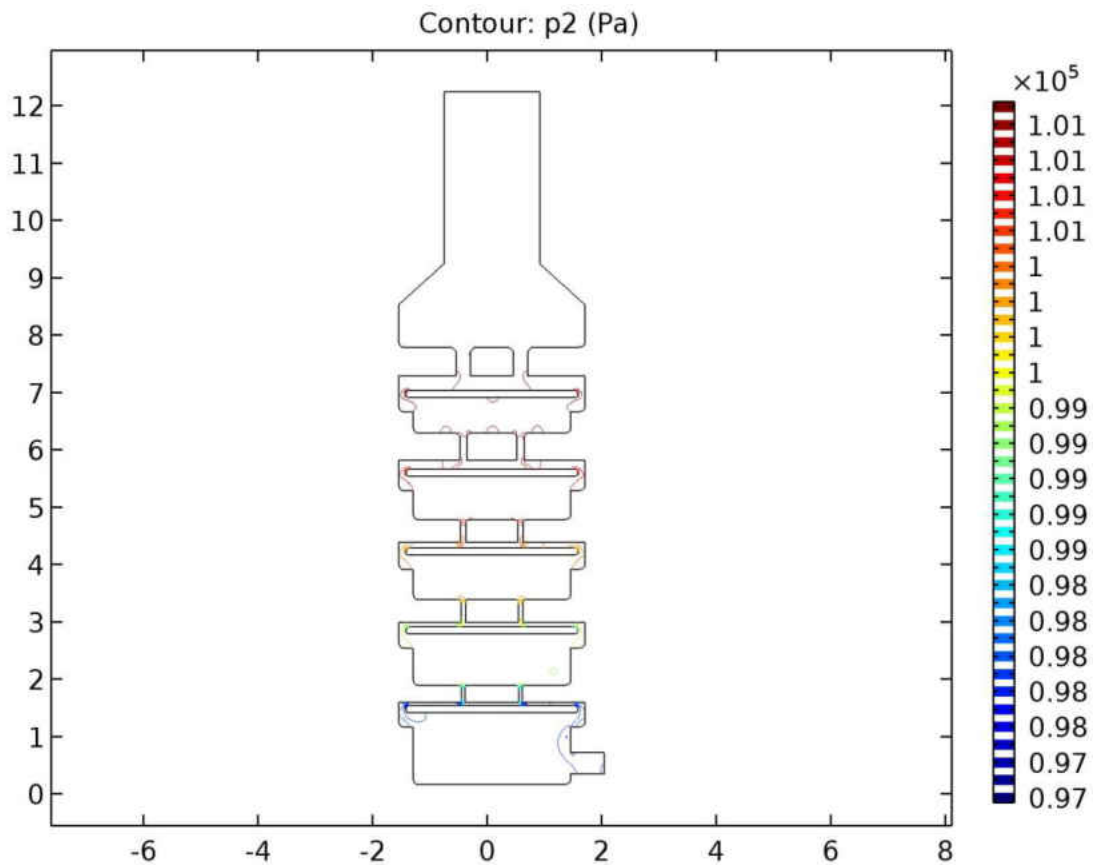
Figure 2.10. Pressure Contour generated by COMSOL.

CHAPTER 3

5-STAGE INERTIAL CASCADE IMPACTOR DESIGN

3.1 Inertial cascade impactor design and manufacture.

Cascade impactors are sophisticated and yet simple devices. They are made of several stages for which the main purpose is separating aerosol particles by their aerodynamic sizes. This is accomplished by producing a vacuum in the cascade impactor body, so that an aerosol sample is forced to flow into it. As this aerosol sample flows into each of the stages of the cascade impactor, it carries suspended particles within it, but when these particles pass through each nozzle, they separate from the aerosol flow and impact the collection plates of each stage, depending on their aerodynamic size.

Inertia is the driving factor that causes this separation; the bigger the particle, the bigger its inertia. Each stage of a cascade impactor is designed to separate particles by their inertia, bigger particles have greater inertia, and therefore will separate from the aerosol flow and impact the collection plate. As the aerosol continues to flow within the stages of the impactor, smaller nozzle diameters will separate smaller particles, and this process repeats until the aerosol reaches its lowest stage, and finally leaves the cascade impactor.

Once the aerosol has been circulated through the cascade impactor, the collection plates are removed from the cascade impactor and sent to a laboratory for analysis of their samples.

The complex flow of an aerosol sample through a cascade impactor contrasts with its relative ease of fabrication and assembling. Each stage can be manufactured in a common machine shop; however, drilling the holes that become the nozzles of each stage can be challenging depending on the smallest size of particles desired to be separated from the flow. The smaller the

aerodynamic diameter of the particles, the smaller the nozzle diameter must be. This dependency could lead a designer to come up with nozzle diameters that are extremely difficult to drill, since there might not be such small drill bits available at a common machine shop. Alternate manufacturing procedures should be utilized in cases like this. This limitation was an important factor considered during the design process of the cascade impactor for this thesis; several iterations were performed, which allowed the diameters of the nozzles to increase, and to decrease the number of nozzles in each stage. After each iteration, the Reynolds numbers in each stage were recalculated to ensure that this parameter was within the recommended design interval ($500 < Re < 3000$). All other features of each stage and the total assembly were manufactured using a lathe, CNC mill, and drill benches.

Additionally, assembling a traditional designed cascade impactor is just a matter of stacking the different stages one over the other, and holding them together using any mechanical means; a set of three springs and three hooks were used for this purpose.

An important consideration when designing cascade impactors is the efficiency of each stage, which can be defined as the percentage of particles collected on each collection plate as a function of their size, according to Marple & Willeke (1967).

Several factors influence the efficiency of a cascade impactor stage. Newton, Raabe & Mokler (1976) mention that the best results are obtained when the following design criteria are met:

$$1 < \frac{S}{W} < 5 \tag{3.1}$$

$$1 < \frac{T}{W} < 5 \tag{3.2}$$

$$500 < Re < 3000 \tag{3.3}$$

where

$S =$ is the distance between the end of the nozzle (also known as jet) to the collection plate in each stage

$T =$ is the nozzle throat length

$W =$ is the diameter of the circular nozzle

An important goal when designing a cascade impactor stage, is to ensure that a 50% efficiency is achieved, at least. This means that 50% of the total particles suspended in the aerosol will be collected on the surface of the collection late, while the other 50% will continue moving down the cascade impactor to the next lower stage.

An important decision taken for designing a cascade impactor in this thesis, was to utilize $\frac{S}{W}$ and $\frac{T}{W}$ ratios that yielded practical and easy dimensions for manufacturing purposes. The initial values for these ratios were chosen to be

$$\frac{S}{W} = 1 \tag{3.4}$$

$$1 \leq \frac{T}{W} \leq 5 \tag{3.5}$$

which were the optimum values suggested by Marple (1970), and by Newton, Raabe & Mokler (1976).

Manufacturing nozzles of significantly small diameters requires the use of highly precise machinery, which becomes a costly and difficult task to accomplish; with this limitation in mind, the effective cutoff aerodynamic resistance diameters were selected in such a way that the

nozzles of each stage had diameters that could easily be fabricated using drill bits which are common in any machine shop.

Another important step in the design process is to determine the number of nozzles necessary to ensure that the desired Reynolds number is maintained in a stage. Marple & Willeke (1967) analyzed this design consideration and came up with a plot that can be used for initial design of a cascade impactor. They came up with Equation 3.6

$$Q = \frac{\pi}{12}\left(\frac{\rho_p}{Stk_{50}}\right)^{\frac{1}{2}}\left(\frac{Re}{\rho}\right)^{\frac{3}{2}} n\mu\sqrt{C}D_{50}$$

(3.6)

where

Q = total volumetric flow rate

ρ_p = particle density

Stk_{50} = Stokes number at 50% efficiency in one stage

Re = Reynolds Number

ρ =air density

μ = air dynamic viscosity

n = number of nozzles in a stage

$\sqrt{C}$ =Cunningham slip correction factor

D_{50} =equivalent aerodynamic radius of a unit density sphere

Marple & Willeke (1967) used Equation 3.6 with the assumption that the density of the particle sampled was $\rho_p = 1\frac{g}{cm^3}$; therefore, it was possible to conclude that $D_p = \sqrt{C}D_p$. Besides,

standard air conditions were also assumed: $\rho = 1.205 \cdot 10^{-3} \frac{g}{cm^3}$ and $\mu = 1.81 \cdot$

$10^{-4} P \left(1\ P = 1 \frac{g}{cm \cdot s}\right)$. This consideration led them to the development of a chart shown in
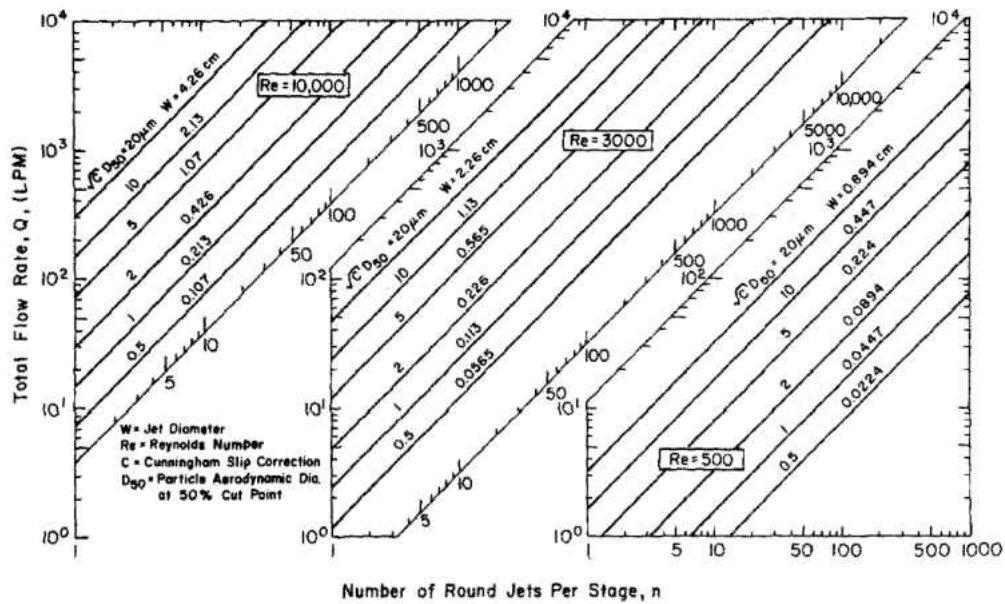
Figure 3.1.

Figure 3.1. Design chart for round impactors. (D_{50} = aerodynamic diameter, at 50% cut point). Marple & Willeke (1967)

During the design process of each stage, it is important to ensure that the Reynolds number is

always within optimal design limits. Since normally each stage requires more than one nozzle to

be present, a relationship between Reynolds number and number of nozzles is required. Marple

& Willeke (1967) recommend Equation 3.7 to be used for this purpose:

$$Re = \frac{\rho V_0 W}{\mu} \tag{3.7}$$

where the velocity in each nozzle can be expressed as

$$V_0 = \frac{4Q}{\pi n W^2} \tag{3.8}$$

Substituting Equation 3.8 into Equation 3.7 yields Equation 3.9

$$Re = \frac{4\rho Q}{\pi n \mu W} \tag{3.9}$$

In this thesis, the optimal design parameters recommended by Marple & Willeke (1967) were approximated, namely $Re = 3000$, since this value of Reynolds number produces the desired 50% efficiency in the Efficiency vs $\sqrt{Stk}$ plot which is the value that our cascade impactor is aiming to. Figure 3.2 shows this relationship. Besides, the ratios $\frac{S}{W} = 1.0$ and $1 \leq \frac{T}{W} \leq 5$ were used, and the total volumetric flow into the cascade impactor was provided by a vacuum pump with a capacity of approximately $40 \frac{l}{min}$ $\left(40,000 \frac{cm^3}{min}\right)$. A high-flow rate pump was chosen in the design of this cascade impactor, to reduce the collection time.

These parameters were used to obtain initial values of nozzle diameters and number of nozzles for each of the five stages in this cascade impactor. It was decided beforehand that the desired particle cutoff diameter for each stage, D_p, was equal to D_{50}, because it was assumed that the particle density equals one. Equation 3.10 states this assumption
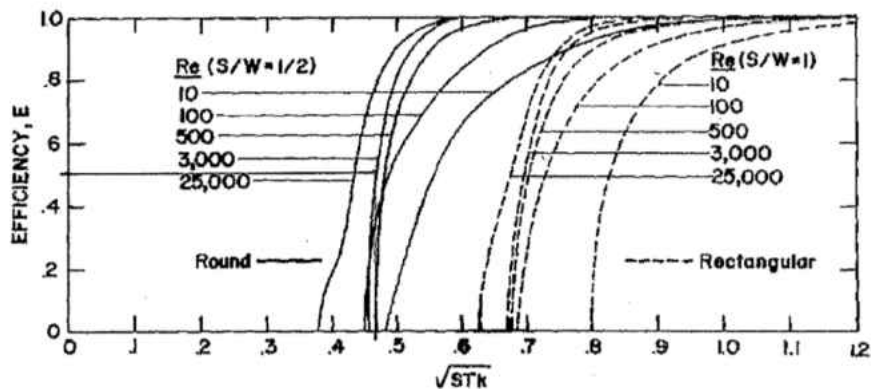
$$\sqrt{C}D_p = \sqrt{C}D_{50} \tag{3.10}$$

Figure 3.2. Theoretical impactor efficiency curves for rectangular and round impactors, both at $\frac{T}{W} = 1$. Marple & Willeke (1967)

3.2 Stage 1 design.

The desired cutoff diameter for stage one is $D_p = 10\mu m$. Figure 3.3 shows the selection of W

and number of nozzles for stage one, applicable to $\sqrt{C}D_p = 10\mu m$, and $Re = 3000$. From this
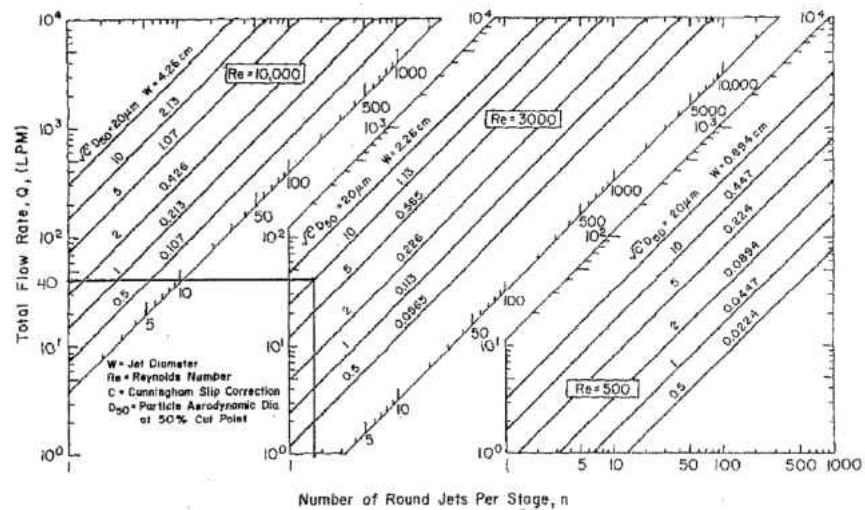
figure, $n \approx 2$, and $W = 1.13\ cm$

Figure 3.3. Selection of Number and Diameter of Nozzles for Stage 1 (Cutoff Diameter 10 μm)

(Marple & Willeke (1967)

The nozzle diameter chosen should be approximated to the closest standard drill bit found in a

common machine shop, for ease of fabrication.

$$W = 1.13\ cm.\frac{1\ inch}{2.54\ cm} = 0.4448\ inch$$

The closest drill bit sizes are $\frac{7}{16}in$ and $\frac{29}{64}in$

$\frac{7}{16}in = 0.4375\ in\frac{2.54\ cm}{1\ in} = 1.111\ cm$

$\frac{29}{64} in = 0.4531\ in\frac{2.54\ cm}{1\ in} = 1.151\ cm$.

Now we will calculate the Reynolds number using these values, and Equation 3.9, to verify that

the Reynolds number criteria still hold:

$$Re = \frac{4\rho Q}{\pi n \mu W} = \frac{4\left(1.205 \cdot 10^{-3}\frac{g}{cm^3}\right)\left(40{,}000\ \frac{cm^3}{min}\right)}{\pi(2)\left(1.81 \cdot 10^{-4}\frac{g}{cm \cdot s}\frac{60\ s}{1\ min}\right)(1.111\ cm)} = 2543$$

$$Re = \frac{4\rho Q}{\pi n \mu W} = \frac{4\left(1.205 \cdot 10^{-3}\frac{g}{cm^3}\right)\left(40{,}000\ \frac{cm^3}{min}\right)}{\pi(2)\left(1.81 \cdot 10^{-4}\frac{g}{cm \cdot s}\frac{60\ s}{1\ min}\right)(1.151\ cm)} = 2454$$

It is observed that both nozzle diameters yield a Reynolds number that complies with the design

requirement $500 < Re < 3000$. A drill bit diameter $\frac{7}{16}in$ could be chosen for stage one, since

this diameter yields the Reynolds number value closest to 3000. However, after performing some

iterations, it can be determined that three nozzles with $W = 0.2559\ in$ (0.65 cm) yield $Re =$

2898. This value is even closer to 3000.

$$Re = \frac{4\rho Q}{\pi n \mu W} = \frac{4\left(1.205 \cdot 10^{-3}\frac{g}{cm^3}\right)\left(40{,}000\ \frac{cm^3}{min}\right)}{\pi(3)\left(1.81 \cdot 10^{-4}\frac{g}{cm \cdot s}\frac{60\ s}{1\ min}\right)(0.65\ cm)} = 2898.$$

The closest drill sizes are Size E $= 0.250\ in$ (0.635 cm) and Size $F = 0.257\ in$ (0.65278 cm).

Once again, it is necessary to verify that the Reynolds number design criteria hold for these new

choices of W:

$$Re = \frac{4\rho Q}{\pi n \mu W} = \frac{4\left(1.205 \cdot 10^{-3}\frac{g}{cm^3}\right)\left(40{,}000\ \frac{cm^3}{min}\right)}{\pi(3)\left(1.81 \cdot 10^{-4}\frac{g}{cm \cdot s}\frac{60\ s}{1\ min}\right)(0.635\ cm)} = 2966.$$

$$Re = \frac{4\rho Q}{\pi n \mu W} = \frac{4\left(1.205 \cdot 10^{-3} \frac{g}{cm^3}\right)\left(40{,}000 \frac{cm^3}{min}\right)}{\pi(3)\left(1.81 \cdot 10^{-4} \frac{g}{cm \cdot s} \frac{60\ s}{1\ min}\right)(0.65278\ cm)} = 2886.$$

Clearly, a drill bit size E provides the closest approximation to $Re = 3000$, so this was the choice. By performing these iterations, it was possible obtain a better distribution of the nozzles, since at first only two nozzles were estimated for stage one, with bigger diameters than after the final iteration. However, it was possible to refine this result after iterating a few more times.

Since it was decided to choose $\frac{S}{W} = 1$ as a design parameter, $s = 0.635\ cm$. Besides utilizing the design criteria $\frac{T}{W} = 2$, then $T = 1.27\ cm$.

The average velocity within any nozzle in stage 1 is calculated using Equation 3.8

$$V_0 = \frac{4Q}{\pi n W^2} = \frac{4\left(40{,}000 \frac{cm^3}{min} \cdot \frac{1\ min}{60s}\right)}{\pi(3)(0.635\ cm)^2} = 702\ \frac{cm}{s} = 7.02\ \frac{m}{s}$$

3.3 Stage 2 design.

Figure 3.4 shows the selection of W and number of nozzles for stage two, applicable to $\sqrt{C}D_p =$

$5\ \mu m$, and $Re = 3000$. From this figure, initial values $n = 3$, and $W = 0.565\ cm$ were chosen.

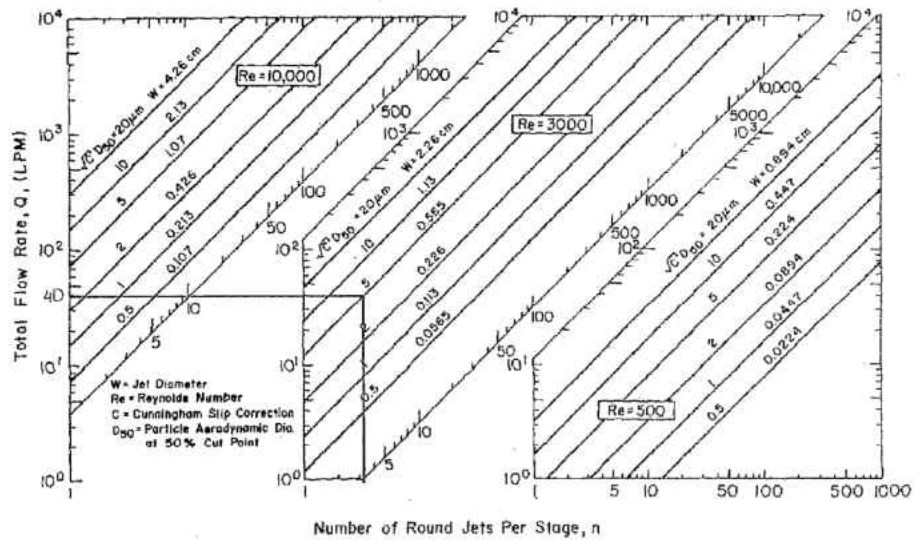
Figure 3.4. Selection of Number and Diameter of Nozzles for Stage 2 (Cutoff Diameter 5 μm)

(Marple & Willeke (1967)

The nozzle diameter chosen should be approximated to the closest standard drill bit found in a

common machine shop, for ease of fabrication.

$$W = 0.565\ cm. \frac{1\ inch}{2.54\ cm} = 0.222\ inch$$

The closest drill bit sizes are Size 2 (0.221 in) and Size 1 (0.228 in).

$$Size\ 2 = 0.221\ in \cdot \frac{2.54\ cm}{1\ in} = 0.5613\ cm\ .$$

$$Size\ 1 = 0.228\ in \cdot \frac{2.54\ cm}{1\ in} = 0.5791\ cm\ .$$

Now we will calculate the Reynolds number using these values, and Equation 3.9, to verify that

the Reynolds number criteria still hold for either drill bit diameter:

$$Re = \frac{4\rho Q}{\pi n \mu W} = \frac{4\left(1.205 \cdot 10^{-3} \frac{g}{cm^3}\right)\left(40{,}000 \frac{cm^3}{min}\right)}{\pi(3)\left(1.81 \cdot 10^{-4} \frac{g}{cm \cdot s} \frac{60\ s}{1\ min}\right)(0.5613\ cm)} = 3355$$

$$Re = \frac{4\rho Q}{\pi n \mu W} = \frac{4\left(1.205 \cdot 10^{-3} \frac{g}{cm^3}\right)\left(40{,}000 \frac{cm^3}{min}\right)}{\pi(3)\left(1.81 \cdot 10^{-4} \frac{g}{cm \cdot s} \frac{60\ s}{1\ min}\right)(0.5791\ cm)} = 3252$$

A drill bit diameter Size 1 (0.228 in) could be chosen for stage one, since this produces the

Reynolds number value closest to 3000. However, it is possible to obtain a better approximation

by performing iterations. For this purpose, both number of nozzles and their diameter were

varied so that a close approximation to $Re = 3000$ was obtained. Finally, it was determined that

5 nozzles with diameter 0.157 in (0.4 cm) yielded $Re = 2825$. A drill bit size 22 (0.157 in) is the

best choice for stage two.

Since we decided to choose $\frac{S}{W} = 1$ as a design parameter, $s = 0.4\ cm$. Besides utilizing the

design criteria $\frac{T}{W} = 3$, then $T = 1.2\ cm$.

The average velocity within any nozzle in stage 2 is calculated using equation 3.8

$$V_0 = \frac{4Q}{\pi n W^2} = \frac{4\left(40{,}000 \frac{cm^3}{min} \cdot \frac{1\ min}{60s}\right)}{\pi(5)(0.4\ cm)^2} = 1061 \frac{cm}{s} = 10.61 \frac{m}{s}$$

3.4 Stage 3 design.

Figure 3.5 shows the selection of W and number of nozzles for stage three, applicable to

$\sqrt{C}D_p = 2\ \mu m$, and $Re = 3000$. From this figure, the initial values $n = 8$, and $W = 0.226\ cm$
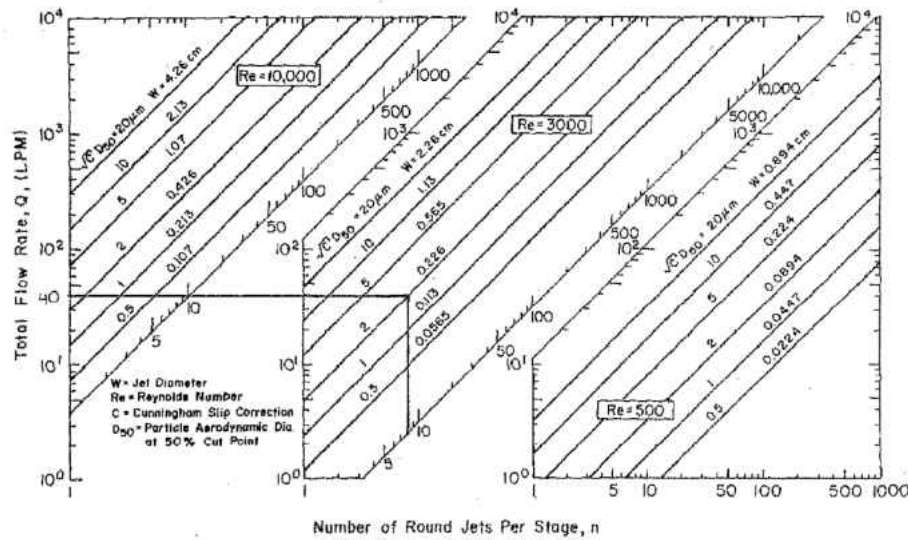
are obtained.

Figure 3.5. Selection of Number and Diameter of Nozzles for Stage 3 (Cutoff Diameter 2 μm)

(Marple & Willeke (1967)

The nozzle diameter chosen should be approximated to the closest standard drill bit found in a

common machine shop, for ease of fabrication.

$$W = 0.226\ cm.\frac{1\ inch}{2.54\ cm} = 0.089\ inch$$

The closest drill bit sizes are Size 43 (0.089 in) and Size 44 (0.086 in)

$Size\ 43 = 0.089\ in \cdot \frac{2.54\ cm}{1\ in} = 0.226\ cm$.

$Size\ 44 = 0.086\ in \cdot \frac{2.54\ cm}{1\ in} = 0.2184\ cm$.

Now we will calculate the Reynolds number using these values, and Equation 3.9, to verify that

the Reynolds number criteria still hold:

$$Re = \frac{4\rho Q}{\pi n \mu W} = \frac{4\left(1.205 \cdot 10^{-3}\ \frac{g}{cm^3}\right)\left(40{,}000\ \frac{cm^3}{min}\right)}{\pi(8)\left(1.81 \cdot 10^{-4}\ \frac{g}{cm \cdot s}\frac{60\ s}{1\ min}\right)(0.226\ cm)} = 3125$$

$$Re = \frac{4\rho Q}{\pi n \mu W} = \frac{4\left(1.205 \cdot 10^{-3}\ \frac{g}{cm^3}\right)\left(40{,}000\ \frac{cm^3}{min}\right)}{\pi(8)\left(1.81 \cdot 10^{-4}\ \frac{g}{cm \cdot s}\frac{60\ s}{1\ min}\right)(0.2184\ cm)} = 3234$$

A drill bit diameter Size 43 (0.089 in) could be chosen for stage one, since this produces the

Reynolds number value closest to 3000. A better approximation was obtained by performing

iterations. For this purpose, both number of nozzles and their diameter were varied so that a close

approximation to $Re = 3000$ was obtained. Finally, it was determined that 8 nozzles with

diameter 0.0984 in (0.25 cm) yielded $Re = 2825$. A drill bit size 40 (0.098 in) is the best choice

for stage three.

Since we decided to choose $\frac{S}{W} = 1$ as a design parameter, $s = 0.25\ cm$. And since $\frac{T}{W} = 4 \rightarrow T = 1.0\ cm$.

The average velocity within any nozzle in stage 3 is calculated using Equation 3.8

$$V_0 = \frac{4Q}{\pi n W^2} = \frac{4\left(40{,}000\ \frac{cm^3}{min} \cdot \frac{1\ min}{60s}\right)}{\pi(8)(0.25\ cm)^2} = 1697\ \frac{cm}{s} = 16.97\ \frac{m}{s}$$

3.5 Stage 4 design.

Figure 3.6 shows the selection of W and number of nozzles for stage four, applicable to $\sqrt{C}D_p =$ 1 μm, and $Re = 3000$. From this figure, the initial values $n = 16$, and $W = 0.113\ cm$ were chosen.
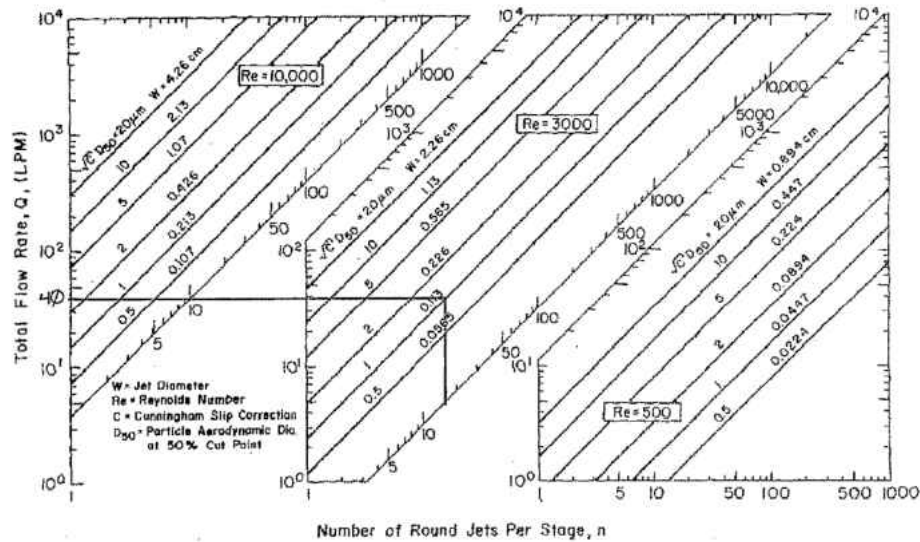

Figure 3.6. Selection of Number and Diameter of Nozzles for Stage 4 (Cutoff Diameter 1 µm)

(Marple & Willeke (1967)

The nozzle diameter chosen should be approximated to the closest standard drill bit found in a common machine shop, for ease of fabrication.

$$W = 0.113\ cm.\frac{1\ inch}{2.54\ cm} = 0.0445\ inch$$

The closest drill bit sizes are Size 57 (0.043 in) and Size 56 (0.0465 in)

$$Size\ 57 = 0.043\ in \cdot \frac{2.54\ cm}{1\ in} = 0.1092\ cm\ .$$

$$Size\ 56 = 0.0465\ in \cdot \frac{2.54\ cm}{1\ in} = 0.1181\ cm\ .$$

Now we will calculate the Reynolds number using these values, and Equation 3.9, to verify that the Reynolds number criteria still hold:

$$Re = \frac{4\rho Q}{\pi n \mu W} = \frac{4\left(1.205 \cdot 10^{-3}\,\frac{g}{cm^3}\right)\left(40{,}000\,\frac{cm^3}{min}\right)}{\pi(16)\left(1.81 \cdot 10^{-4}\,\frac{g}{cm \cdot s}\,\frac{60\,s}{1\,min}\right)(0.1092\,cm)} = 3234$$

$$Re = \frac{4\rho Q}{\pi n \mu W} = \frac{4\left(1.205 \cdot 10^{-3}\,\frac{g}{cm^3}\right)\left(40{,}000\,\frac{cm^3}{min}\right)}{\pi(16)\left(1.81 \cdot 10^{-4}\,\frac{g}{cm \cdot s}\,\frac{60\,s}{1\,min}\right)(0.1181\,cm)} = 2991$$

A drill bit Size 56 could be chosen for stage one, since this produces the Reynolds number value closest to 3000. Even though this is a good approximation, the nozzle diameter is so small, it is more convenient to perform iterations that yield a bigger diameter to facilitate manufacturing. After performing a few iterations, it was found that 10 nozzles with diameter 0.2 cm (0.07874 in) was an optimal selection. Even though the number of nozzles decreased, the resultant Reynolds number was 2825, which is still reasonably close to 3000. A drill bit number 47 (0.0781 in) is a good choice for stage four, yielding a Reynolds number of 2854, which is very close to 2825.

Since it was decided to choose $\frac{S}{W} = 1$ as a design parameter, $s = 0.2\,cm.$ and $\frac{T}{W} = 5 \rightarrow T = 1.0\,cm.$

The average velocity within any nozzle in stage 4 is calculated using Equation 3.8

$$V_0 = \frac{4Q}{\pi n W^2} = \frac{4\left(40{,}000\,\frac{cm^3}{min} \cdot \frac{1\,min}{60s}\right)}{\pi(10)(0.2\,cm)^2} = 2157\,\frac{cm}{s} = 21.57\,\frac{m}{s}$$

3.6 Stage 5 design.

Figure 3.7 shows the selection of W and number of nozzles for stage five, applicable to $\sqrt{C}D_p =$
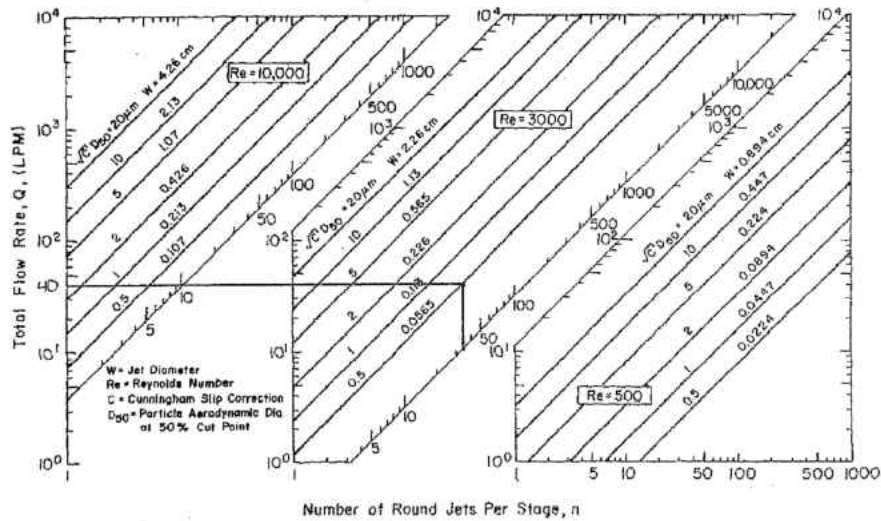0.5 μm, and $Re = 3000$. From this figure, the initial values $n = 36$, and $W = 0.0565\ cm$ were
obtained.

Figure 3.7. Selection of Number and Diameter of Nozzles for Stage 5 (Cutoff Diameter 0.5 μm)

(Marple & Willeke (1967)

The nozzle diameter chosen should be approximated to the closest standard drill bit found in a
common machine shop, for ease of fabrication.

$$W = 0.0565\ cm.\frac{1\ inch}{2.54\ cm} = 0.022\ inch$$

The closest drill bit sizes are Size 75 (0.021 in) and Size 74 (0.0225 in).

$Size\ 75 = 0.021\ in \cdot \frac{2.54\ cm}{1\ in} = 0.0533\ cm$.

$Size\ 74 = 0.0225\ in \cdot \frac{2.54\ cm}{1\ in} = 0.05715\ cm$.

Now we will calculate the Reynolds number using these values, and Equation 3.9, to verify that the Reynolds number criteria still hold:

$$Re = \frac{4\rho Q}{\pi n \mu W} = \frac{4\left(1.205 \cdot 10^{-3}\frac{g}{cm^3}\right)\left(40{,}000\frac{cm^3}{min}\right)}{\pi(36)\left(1.81 \cdot 10^{-4}\frac{g}{cm \cdot s}\frac{60\ s}{1\ min}\right)(0.0533\ cm)} = 2945$$

$$Re = \frac{4\rho Q}{\pi n \mu W} = \frac{4\left(1.205 \cdot 10^{-3}\frac{g}{cm^3}\right)\left(40{,}000\frac{cm^3}{min}\right)}{\pi(36)\left(1.81 \cdot 10^{-4}\frac{g}{cm \cdot s}\frac{60\ s}{1\ min}\right)(0.05715\ cm)} = 2747$$

A drill bit Size 75 could finally be chosen for stage one, since this produces the Reynolds number value closest to 3000. However, even though the previous results are obtained from direct use of the criteria recommended by Marple & Willeke (1967), manufacturing such small diameter nozzles is challenging. Therefore, more iterations were performed, resulting in only 13 nozzles, which have a diameter of $W = 0.15\ cm$ (0.059 in), resulting in $Re = 2898$. A drill bit size 53 (0.0595 in) is a good choice for stage 5.

Since it was decided to choose $\frac{S}{W} = 1$ as a design parameter, $s = 0.15\ cm$, and $\frac{T}{W} = 5$; therefore $T = 0.75\ cm$.

The average velocity within any nozzle in stage 5 is calculated using Equation 3.8

$$V_0 = \frac{4Q}{\pi n W^2} = \frac{4\left(40{,}000\frac{cm^3}{min} \cdot \frac{1\ min}{60s}\right)}{\pi(13)(0.15\ cm)^2} = 2902\ \frac{cm}{s} = 29.02\ \frac{m}{s}$$

Table 3.1 summarizes the design results obtained in this section. It is important to note that the $\frac{T}{W}$ ratios were chosen in such a way to ease the manufacturing process of each stage. This ratio was

chosen to be in the range $1 \leq \frac{T}{W} \leq 5$. The same idea was applied to select the most appropriate

nozzle diameter for each stage, which resulted in less nozzles in each stage, but bigger diameters.

Stage	Cutoff Diameter (µm)	Number of nozzles	Nozzle Diameter W $(\cdot 10^{-2} m)$	Nozzle Throat Length T $(\cdot 10^{-2} m)$	Nozzle to plate distance S $(\cdot 10^{-2} m)$	Nozzle area $(\cdot 10^{-6} \, m^2)$	Air velocity in nozzle $\left(\frac{m}{s}\right)$	Reynolds Number
1	10	3	0.635	1.27	0.635	31.67	7.02	2966
2	5	5	0.4	1.2	0.4	12.57	10.61	2825
3	2	8	0.25	1.0	0.25	4.91	16.97	2825
4	1	10	0.2	1.0	0.2	3.14	21.57	2825
5	0.5	13	0.15	.75	0.15	1.77	29.02	2898

Table 3.1. Summary of design parameters

Another important factor considered in the design of cascade impactors is the spatial distribution

of the nozzles on each stage. Kwon, Kim, & Lee. (2002) concluded that the optimal nozzle array

for a cascade impactor is obtained using the Model 5 configuration, shown in Figure 3.8. This

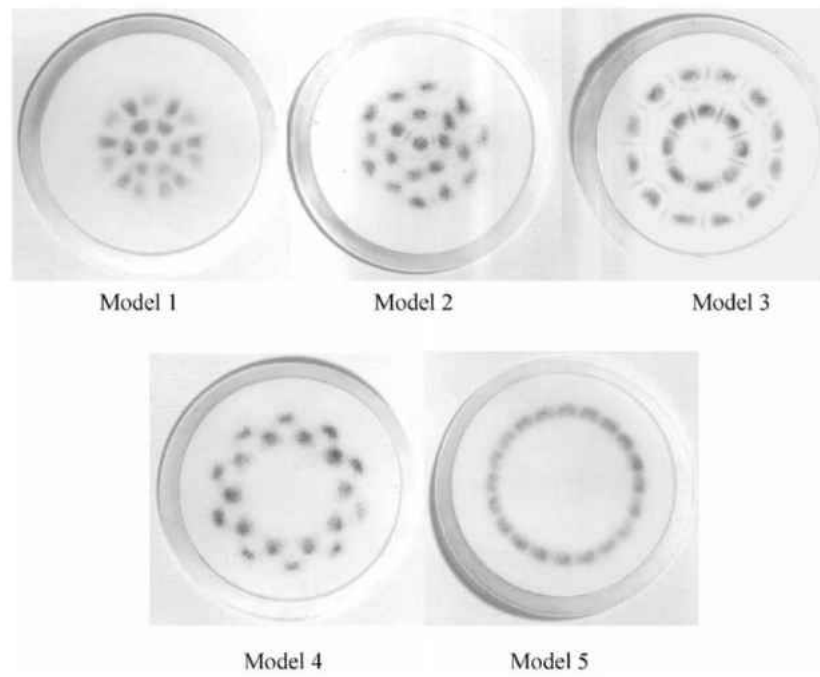was the model used to distribute the nozzle holes on each plate for this study.

Figure 3.8. Nozzle array models for cascade impactor design. Kwon, Kim, & Lee. (2002).

3.7 Inertial cascade impactor manufacture.

There are several design impactor designs in the market. For example, the company Copley
Scientific uses stainless steel and aluminum for their designs. Aluminum 6063 was used for the
design of the cascade impactor in this thesis. This material was chosen due to its ease of
machineability as well as its smooth surfaces after machining. A 4-inch, 16-inch long round
stock of aluminum 6063 was reduced to a 3.750-in diameter, which is the outer diameter of each
stage.

After reaching this final diameter, the round stock was cut into five pieces used for
manufacturing the stages, one piece to manufacture the base of the cascade impactor, and one
piece to manufacture the inlet cone. A CNC milling machine was used to carve each of the stage
pieces, and a drill bench to drill the holes that became the stages nozzles. The cascade impactor
stages, collection plates and inlet cone where manufactured at ODU's machine shop. Figure 3.9
shows the cascade impactor base as it was being manufactured. A set of springs hooks and bolts
was used to compress the inertial cascade impactor stages to improve airtightness of the device.
For this purpose, O-rings were installed on the outer surface in-between each stage; additionally,
one O-ring was installed at the interface between the inlet cone and stage 1.

Approximately 30-man-hours were required to completely manufacture the inertial cascade
impactor at the machine shop at ODU, once it was possible for their technicians to start working
on it. Figures 3.10 and 3.11 show pictures of different components of the cascade impactor after
manufacturing. Figures 3.12 and 3.13 show the complete inertial cascade impactor.

Figure 3.9. Manufacturing base on CNC milling machine

Figure 3.10. Assembled base

Figure 3.11. Several parts manufactured on CNC milling machine

Figure 3.12. Inertial cascade impactor after leaving the machine shop.

Figure 3.13. Fully assembled Inertial cascade impactor

3.8 Total cost.

The total cost of the materials purchased to manufacture the inertial cascade impactor was USD 292.45. Table 3.2 shows the break-down of this total.

Material	Amount	Dimensions	Price (USD)
Aluminum Sheet 5052H32	1	12 in x 24 in, $\frac{1}{8}$in thick	48.61
Aluminum round bar 6061T6511	1	4 in diameter, 16 in length	99.29
Vacuum Pump	1	1.5 CFM	89.34
Vinyl Tube	1	$\frac{1}{2}$ OD X $\frac{3}{8}$ $IDX10\ ft$	4.93
Brass Pipe Nipple	1	$\frac{1}{8}X\ 1\frac{1}{2}$	3.54
Hexagonal Bolt	3	$\frac{1}{4}X\ \frac{3}{4}$	0.36
Square O-ring (AS568-237)	5	3.375ID, 3.625OD, 0.125CS	5.05 + 0.55 + 6.13 (shipping) = 11.63
O-ring (AS568-041)	5	3.0 ID, 3,125OD, 1/16 CS	
Extension Spring	3	0.25OD, 4.75 in. long	8.24
Steel Hooks	3	0.25D x 4.25 in long	3.12
Petri Dishes	20	3.642D x 0.590 height	17.26

Table 3.2. Inertial cascade impactor costs of material

Figure 3.14 through Figure 3.22 show the blueprints of the cascade impactor designed in this
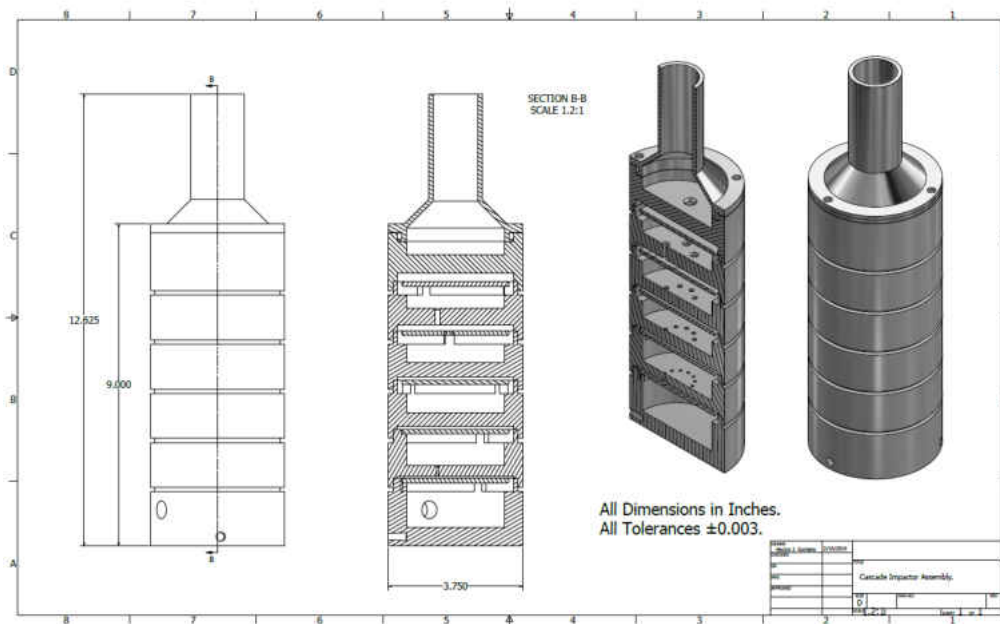
thesis.

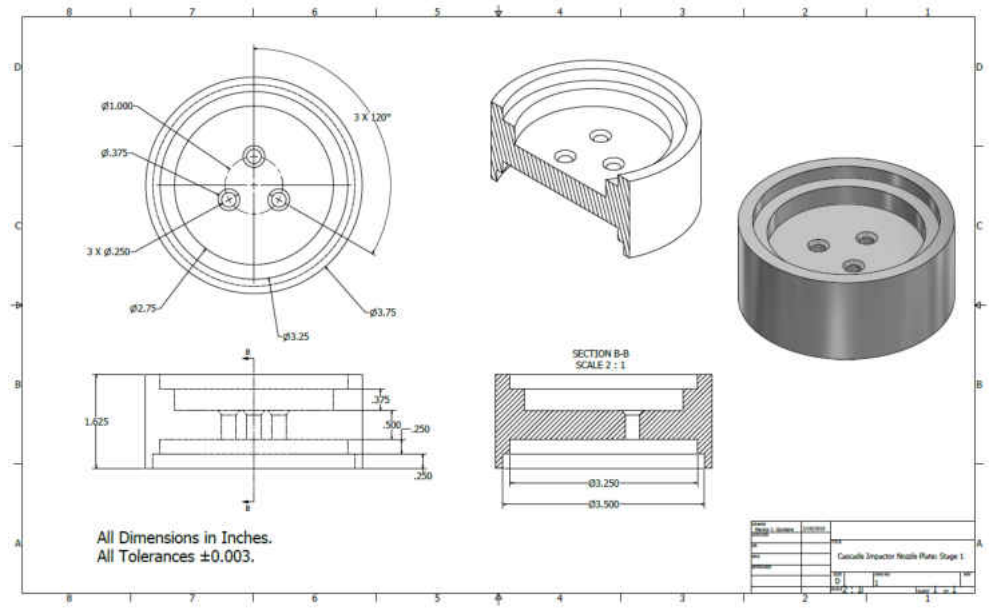Figure 3.14. Cascade Impactor Assembly

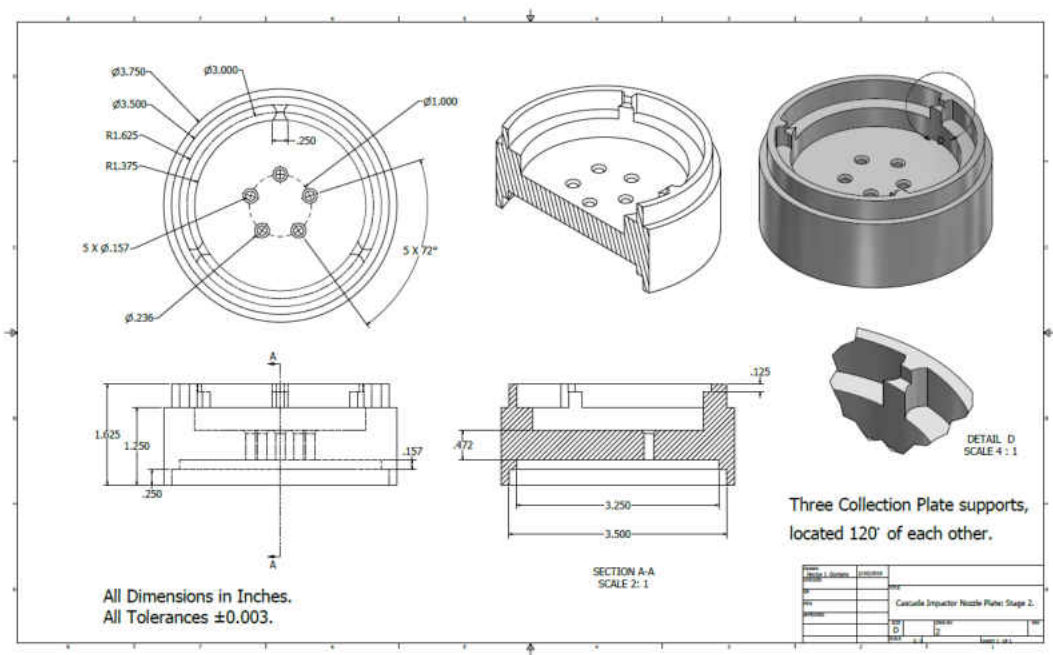Figure 3.15. Cascade Impactor Stage 1.
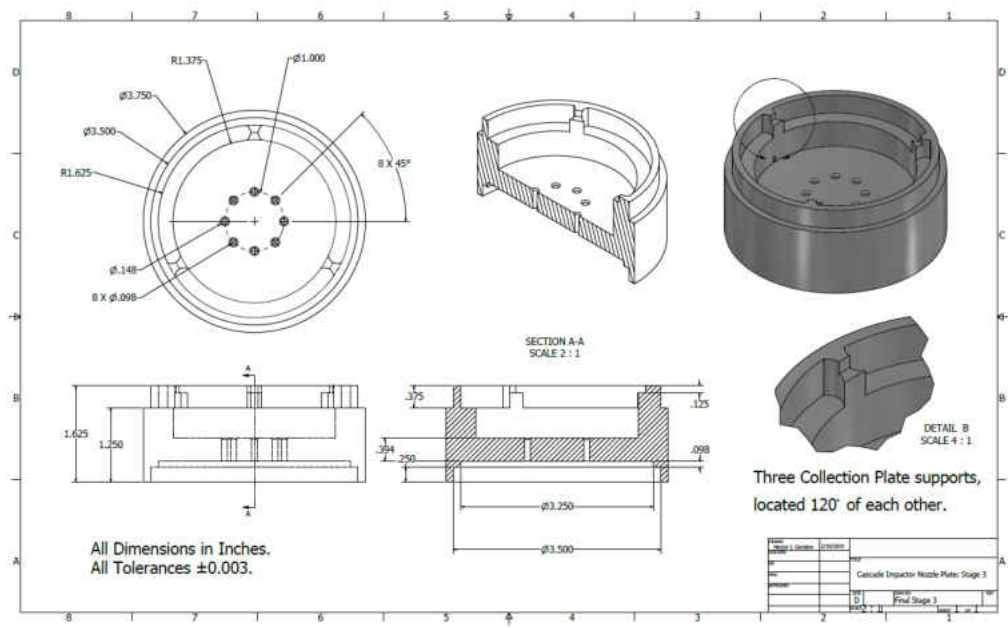

Figure 3.16. Cascade Impactor Stage 2.

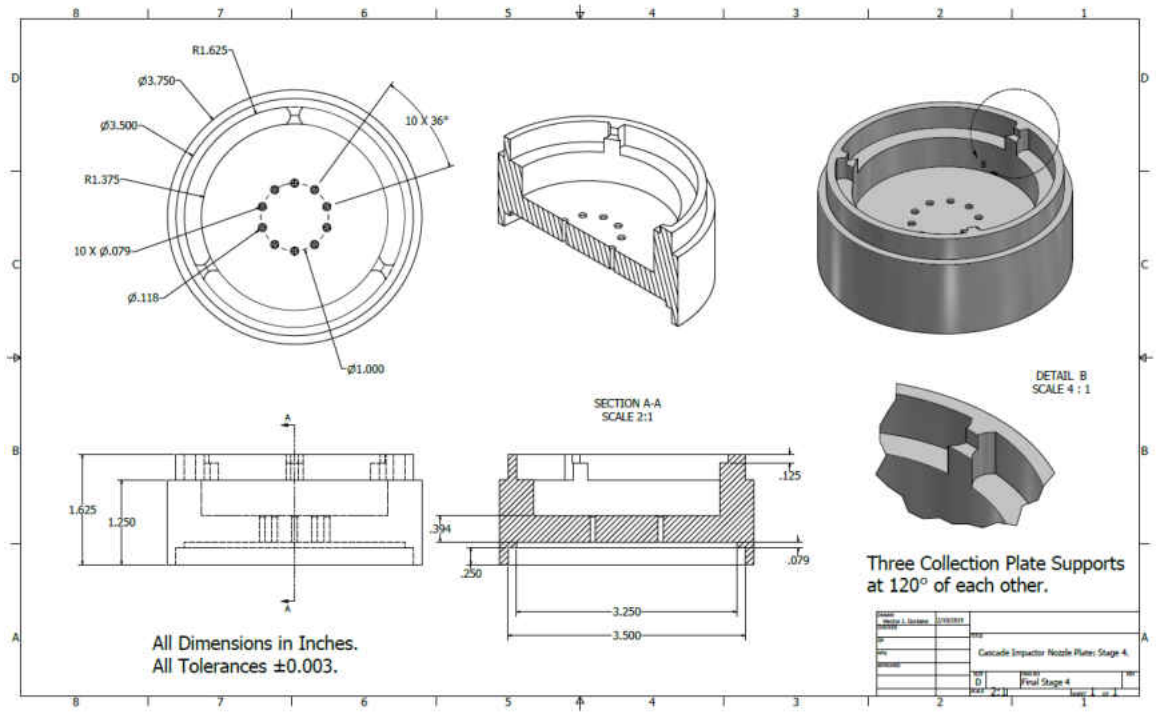Figure 3.17. Cascade Impactor Stage 3.

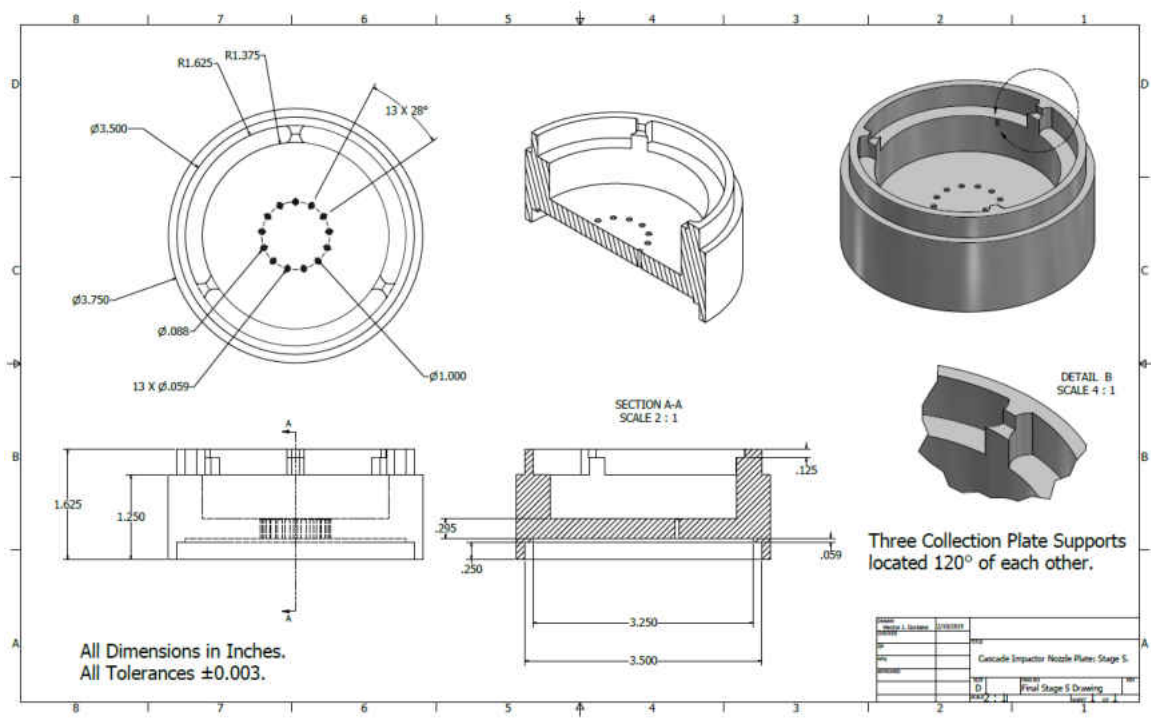Figure 3.18. Cascade Impactor Stage 4.

55

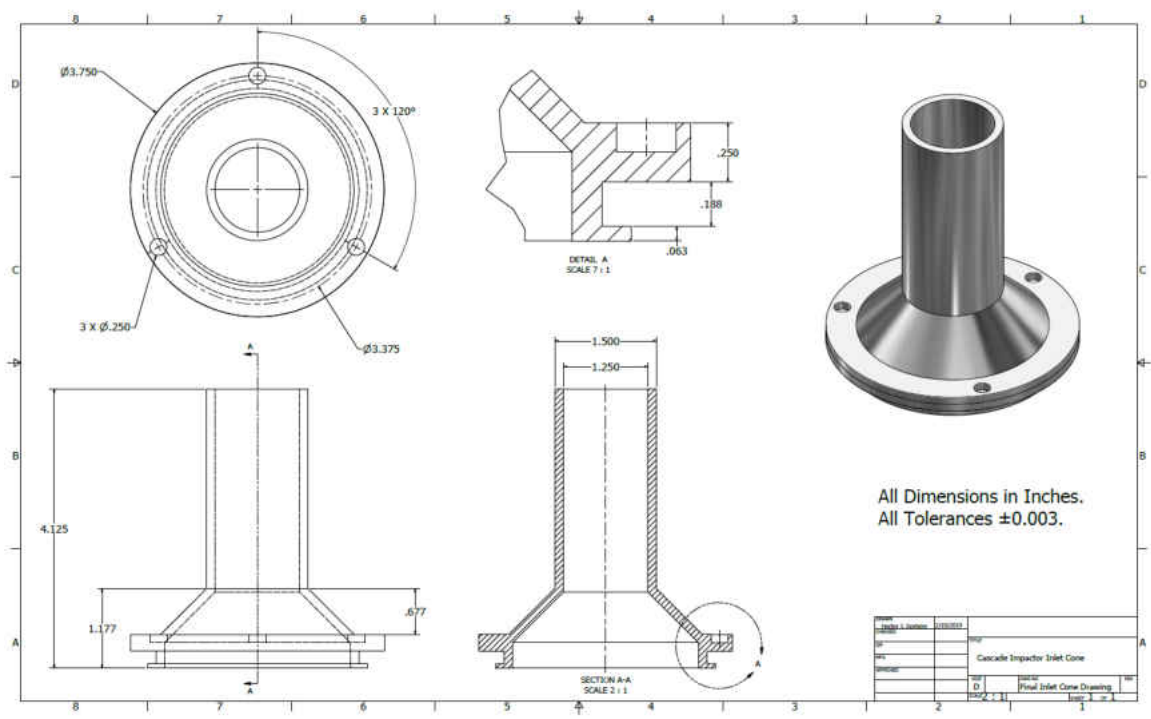Figure 3.19. Cascade Impactor Stage 5.

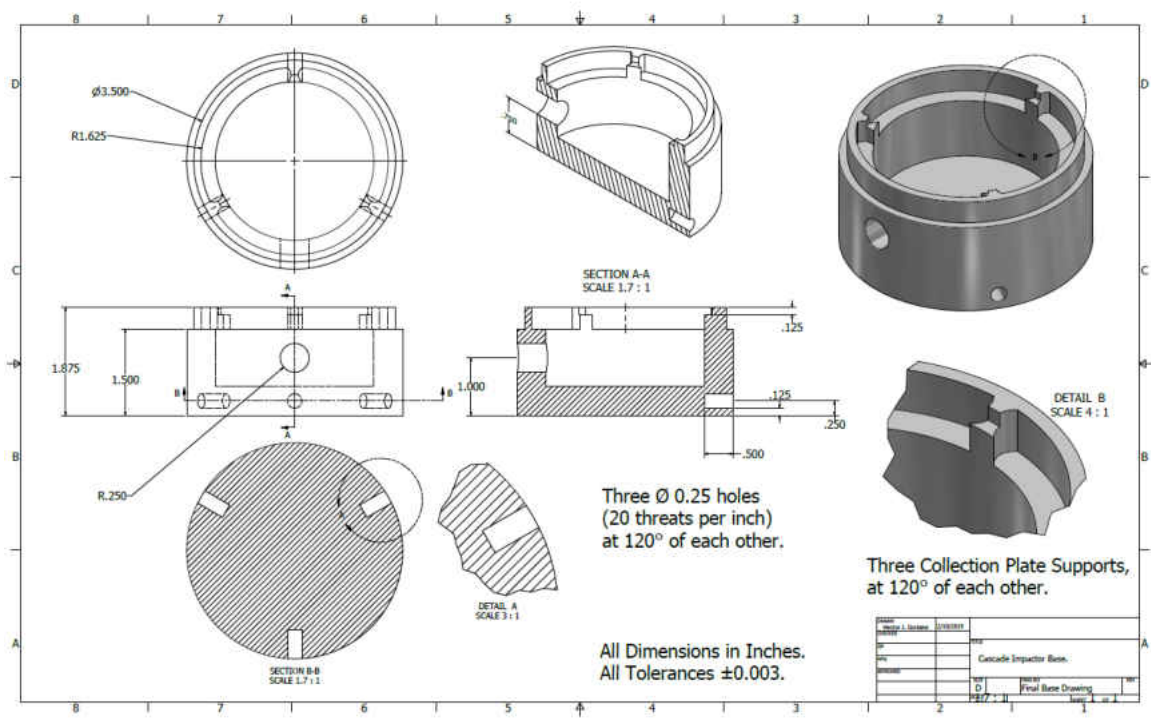Figure 3.20. Cascade Impactor Inlet Cone.
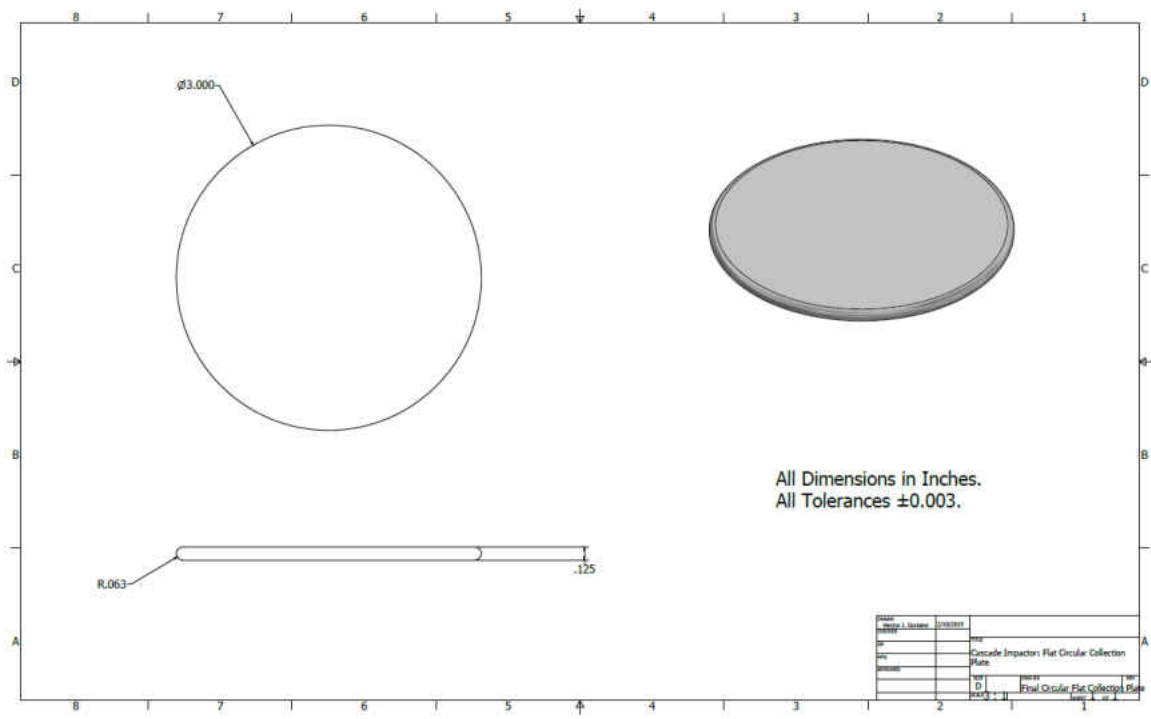
Figure 3.21. Cascade Impactor Base.

Figure 3.22. Cascade Impactor Collection Plate

CHAPTER 4

EXPERIMENTS

4.1 Sample collection experiment.

After the inertial cascade impactor was manufactured, two air samples were collected in order to determine whether the distribution of particulate matter in each stage complies with the design goals. The designed cutoff diameter for each stage is shown in table 4.1

Stage	Cutoff Diameter (µm)
1	10
2	5
3	2
4	1
5	0.5

Table 4.1. Cutoff diameter for each stage

4.2 Experiment set-up.

Once the inertial cascade impactor was manufactured and assembled, a 1.5 CFM-vacuum pump was connected to it by a clear plastic flexible tube. This set-up is shown in Figure 4.1. After setting up, the cascade impactor was used to collect two air samples. In order to take the first air sample, the cascade impactor was run for a 24-hour period, collecting the sample from one street in Norfolk, VA.
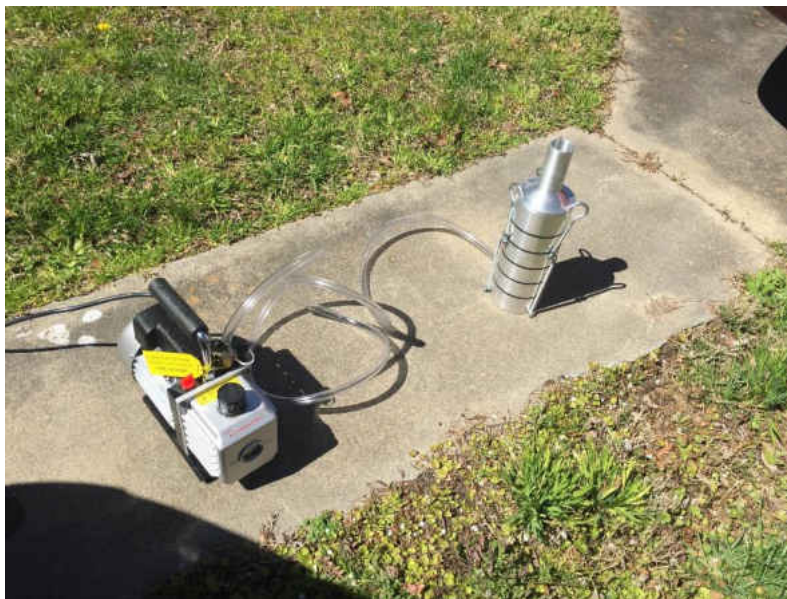
Figure 4.1. Experiment set-up.

This first experiment was used mainly as an initial check of the cascade impactor. Each

collection plate on each stage of the cascade impactor was covered by a 3-in piece of wax paper

so that the particulate matter could deposit on it. After running the cascade impactor for the time

required, it was taken apart, so that the particles collected in each stage could be retrieved. Figure

4.2 shows this process. These contents were taken under a microscope for image capturing and

analysis. Figures 4.3 through 4.7 show the images captured by the microscope by stage. It is

important to note that most of the particulate matter was collected in the lower stages, that is

stages 4 and 5, and most of these particles can be assumed to be smaller than 1 μm if compared

to the scale shown on each picture. Stages 1 and 2 collected the larger particles, as expected. It

was also observed that stage 3 collected particles clearly larger than 2 μm. This could be the

result of these particles bouncing in the upper stages. The small number of particles collected in

each stage could also be the result of this issue.

Figure 4.2.a. Disassembling the inertial cascade impactor to retrieve samples.

Figure 4.2.b. Collecting sample.

Figure 4.2.c. Collecting sample.

Figure 4.2.d. All samples collected.

Figure 4.2. Collection of samples.

Figure 4.3.a

Figure 4.3.b

Figure 4.3.c

Figure 4.3.d

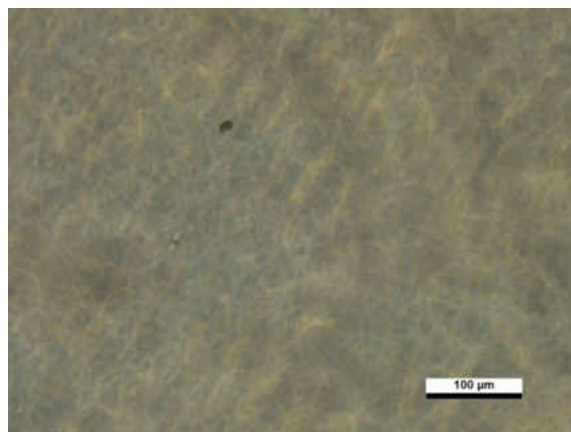Figure 4.3. Images of particulate matter collected on stage 1.

Figure 4.4.a

Figure 4.4.b

Figure 4.4. Images of particulate matter collected on stage 2.

Figure 4.5.a

Figure 4.5.b

Figure 4.5. Images of particulate matter collected on stage 3.
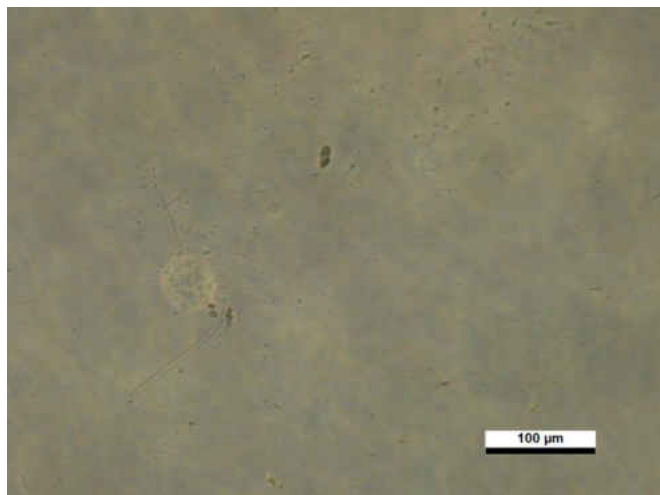
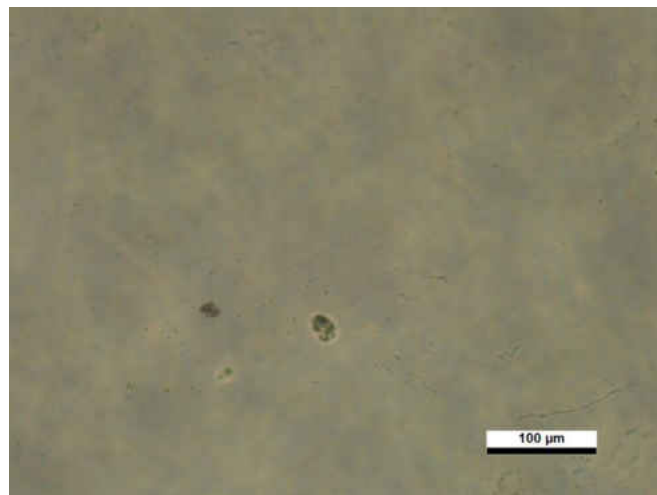Figure 4.6.a   Figure 4.6.b
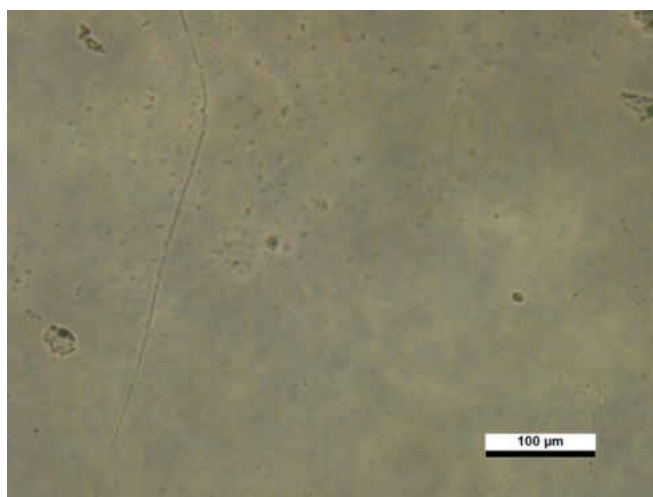

Figure 4.6.c

Figure 4.6. Images of particulate matter collected on stage 4.
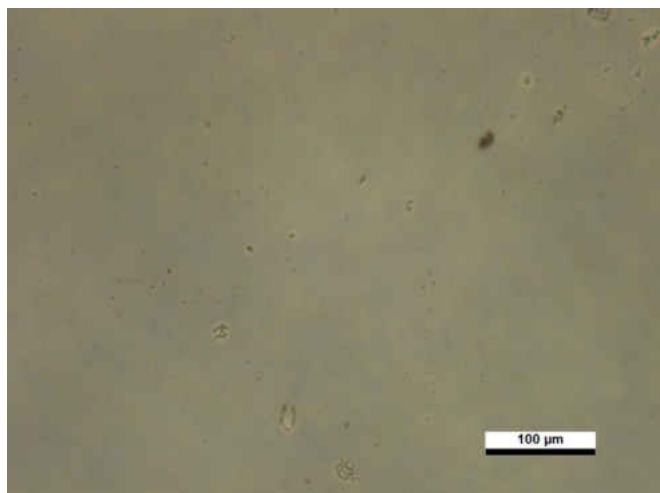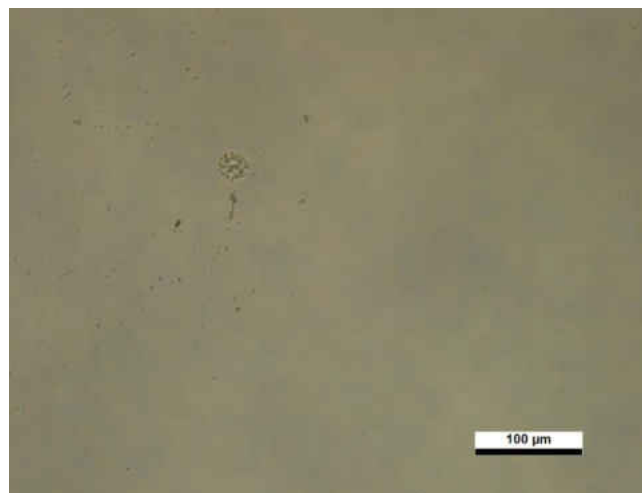
Figure 4.7.a   Figure 4.7.b

Figure 4.7.c

Figure 4.7. Images of particulate matter collected on stage 5.

The air sample in the second experiment was taken during a period of 60 hours to increase the

number of particles to be collected. Besides, oil was applied to each wax paper located on each

stage, to help particles to stick better once they impinge on them. Each circular piece of wax

paper was weighed on a scale before and after the collection of particulate matter. This was done

so that the concentration of particulate matter could be calculated. Figures 4.8.a-e show the

samples collected in each stage.

Figure 4.8.a. Stage 1 collected sample.

Figure 4.8.b. Stage 2 collected sample.

Figure 4.8.c. Stage 3 collected sample.

Figure 4.8.d. Stage 4 collected sample.

Figure 4.8.e. Stage 5 collected sample.

Table 4.2 shows the weight of each wax paper on each collection plate, before and after the

collection.

Stage	Weight before sampling (mg)	Weight after sampling (mg)	Weight Difference (mg)
1	579.2	619.5	40.3
2	582.4	618.1	35.7
3	579.9	617.4	37.5
4	579.9	603.3	23.4
5	588.9	639.2	50.3
Totals	2910.3	3097.5	187.2

Table 4.2. Weight of circular wax paper pieces before and after collection during experiment 2

The total air mass that flowed through the inertial cascade impactor can be calculated as follows:

$$\dot{Q} = 7.08 \cdot 10^{-4} \ \frac{m^3}{s}$$

$$t = 60 \ h. \frac{3600 \ s}{1 \ h} = 2.16 \cdot 10^5 \ s$$

$$\rho = 1.205 \cdot 10^{-3} \frac{g}{cm^3} \cdot \frac{1\ kg}{1000\ g} \cdot \left(\frac{100\ cm}{1\ m}\right)^3 = 1.205\ \frac{kg}{m^3}$$

$$\rho = \frac{\dot{m}}{\dot{Q}} = \frac{m}{\dot{Q}t} \rightarrow m = \dot{Q}\rho t$$

$$m = \dot{Q}\rho t = \left(7.08 \cdot 10^{-4}\ \frac{m^3}{s}\right)\left(1.205\ \frac{kg}{m^3}\right)(2.16 \cdot 10^5\ s)$$

$$m = 184.3\ kg$$

Therefore, 184.3 kg of air flowed through the inertial cascade impactor during the 60 hours it operated continuously. Since the total dust collected on the collection plates was $1.872 \cdot 10^{-6}\ kg$, it is possible to conclude that the concentration of dust in the location where the sample was taken is approximately

$$C_{dust} \approx \frac{1.872 \cdot 10^{-6}\ kg_{dust}}{184.3\ kg_{air}} \approx 1.015 \cdot 10^{-8}\ \frac{kg_{dust}}{kg_{air}}$$

It is important to mention that this calculation does not include wall losses. Figures 4.9 through 4.13 show the image captures obtained from the microscope, for the sample collected on each stage during the second experiment.

Figure 4.9.a. Microscope Image capture of particulate matter collected in Stage 1.

Figure 4.9.b. Microscope Image capture of particulate matter collected in Stage 1.

Figure 4.9.c. Microscope Image capture of particulate matter collected in Stage 1.

Figure 4.10.a. Microscope Image capture of particulate matter collected in Stage 2.

Figure 4.10.b. Microscope Image capture of particulate matter collected in Stage 2.

Figure 4.10.c. Microscope Image capture of particulate matter collected in Stage 2.

Figure 4.11.a. Microscope Image capture of particulate matter collected in Stage 3.

Figure 4.11.b. Microscope Image capture of particulate matter collected in Stage 3.

Figure 4.11.c. Microscope Image capture of particulate matter collected in Stage 3.
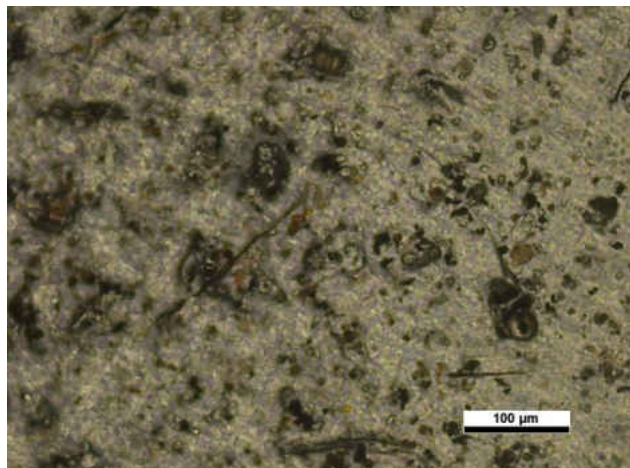
Figure 4.12.a. Microscope Image capture of particulate matter collected in Stage 4.
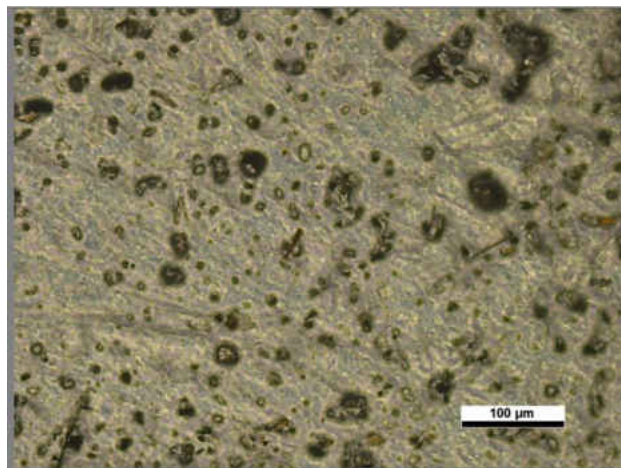

Figure 4.12.b. Microscope Image capture of particulate matter collected in Stage 4.

Figure 4.12.c. Microscope Image capture of particulate matter collected in Stage 4.

Figure 4.13.a. Microscope Image capture of particulate matter collected in Stage 5.
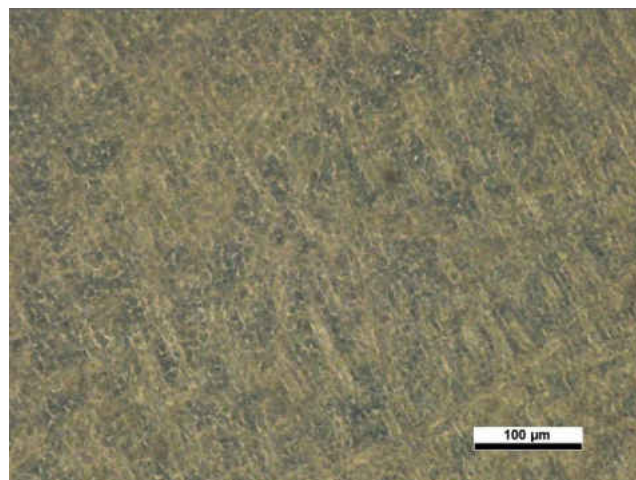
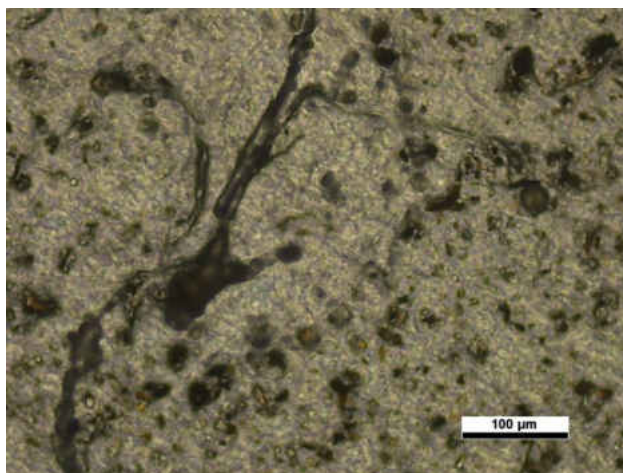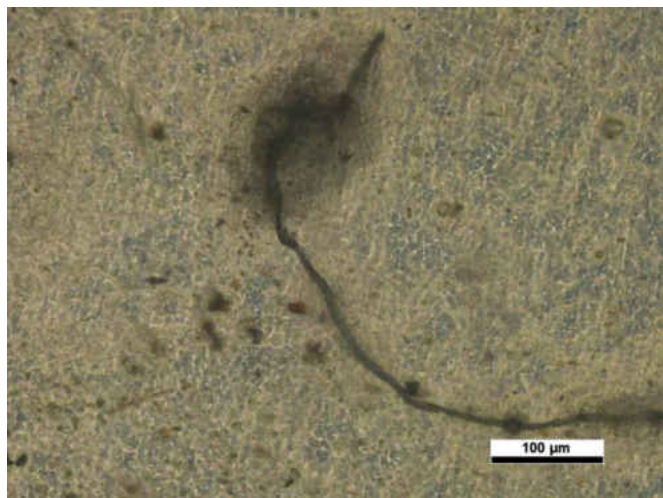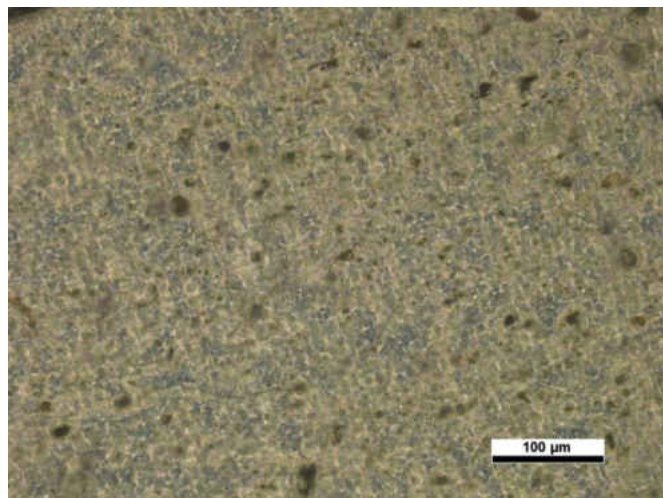Figure 4.13.b. Microscope Image capture of particulate matter collected in Stage 5.
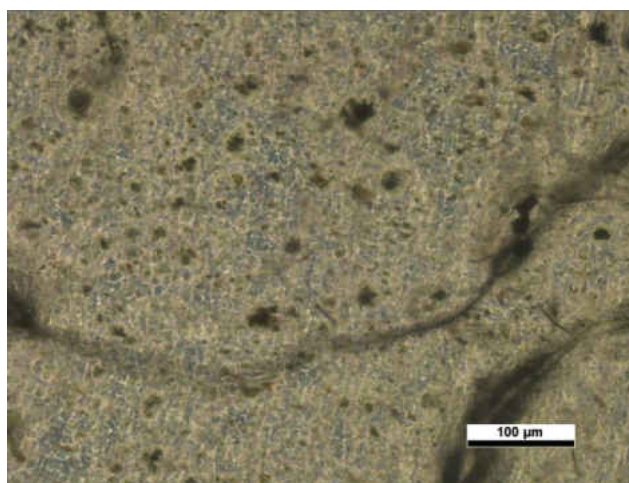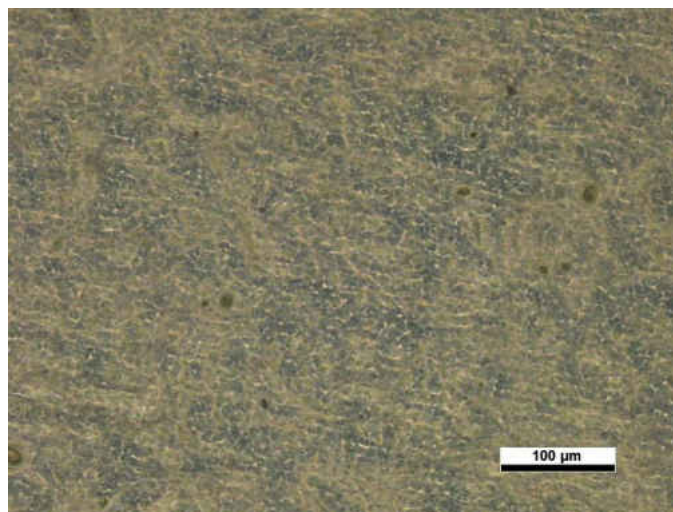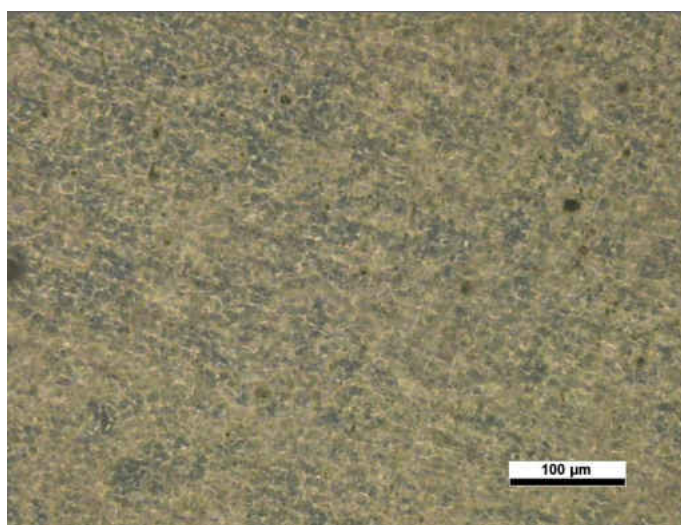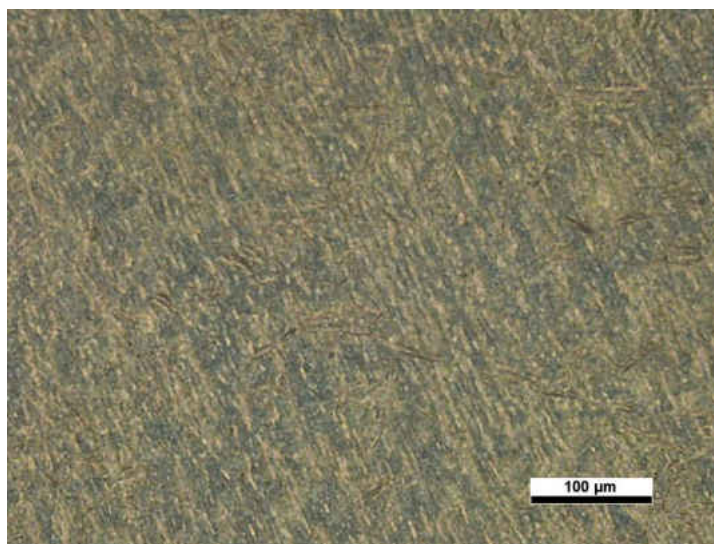

Figure 4.13.c. Microscope Image capture of particulate matter collected in Stage 5.
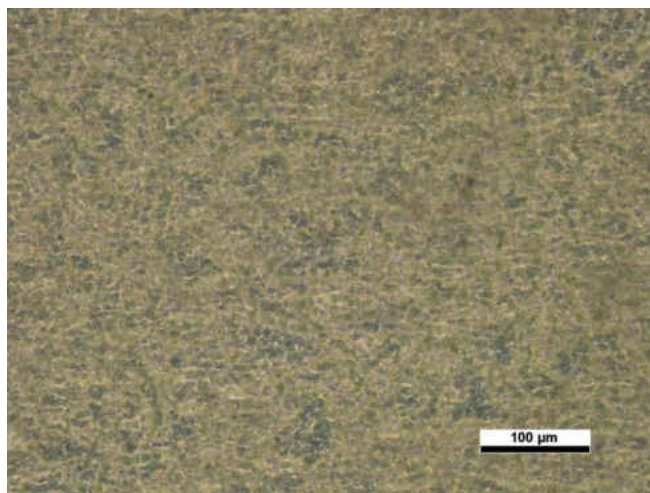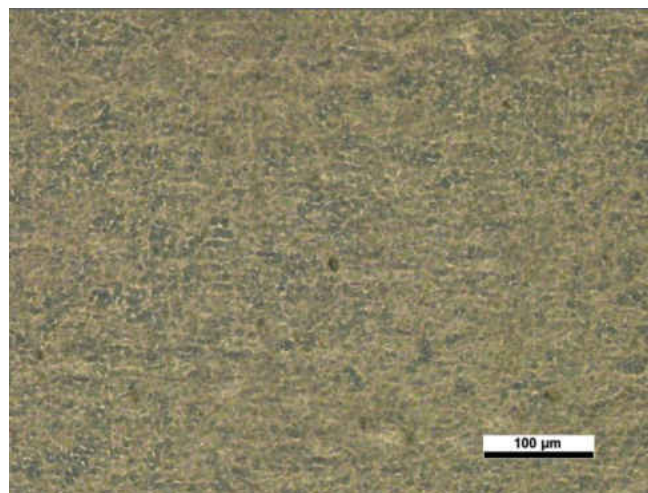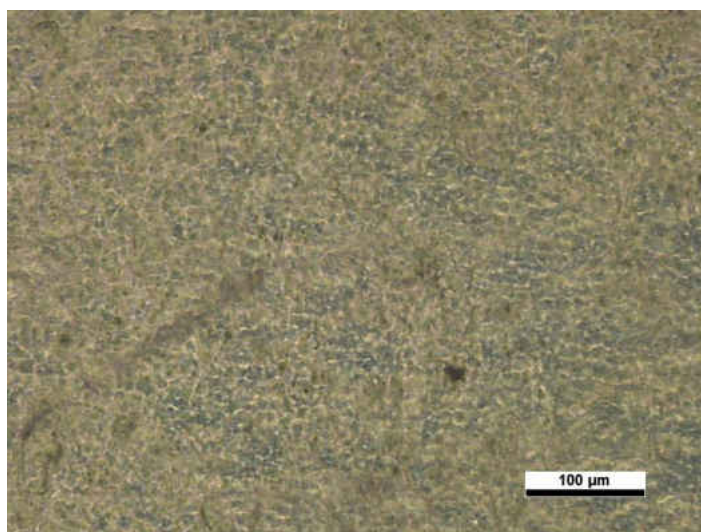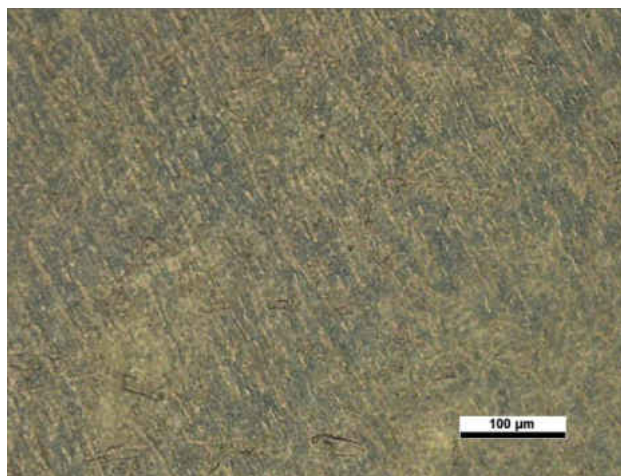
Table 4.3 shows the approximate sizes of 35 particles measured from sample two. It can be

observed that the average size for each stage falls within the expected stage cutoff size.

NUMBER	STAGE 1	STAGE 2	STAGE 3	STAGE4	STAGE 5
1	37.853	5.822	5.018	0.92	1.55
2	19.121	8.274	3.787	1.301	0.775
3	7.889	4.198	1.738	1.2	0.517
4	6.618	6.297	1.738	1.2	0.517
5	5.321	17.858	2.959	0.92	0.258
6	4.134	8.886	2.266	1.235	1.034
7	11.28	4.238	2.093	0.92	0.578
8	8.905	6.078	1.602	1.301	0.817
9	5.343	5.822	1.943	0.873	0.365
10	5.376	9.094	2.748	1.164	0.932
11	6.531	5.008	1.099	1.455	0.775
12	6.769	7.364	1.099	1.2	0.517
13	7.222	4.801	1.738	1.2	0.817
14	4.786	2.911	1.166	1.164	0.775
15	10.686	6.509	2.72	1.455	0.775
16	9.387	9.037	1.166	0.873	1.096
17	5.474	5.851	4.057	1.484	0.578
18	8.396	9.548	2.72	1.164	0.775
19	4.637	8.732	2.488	0.873	0.775
20	8.925	7.59	1.943	1.2	0.775
21	8.905	7.082	2.093	0.873	1.292
22	16.623	7.294	2.332	0.873	1.118
23	12.966	9.879	2.959	1.049	1.5
24	8.562	7.106	6.23	0.92	1.667
25	9.573	5.272	1.229	1.77	0.667
26	33.087	5.272	3.109	1.2	1
27	14.854	8.15	3.886	1.301	0.667
28	8.269	5.851	1.602	0.873	1.054
29	7.741	5.008	1.602	1.567	0.745
30	3.462	5.994	1.943	2.058	0.667
31	8.075	4.801	3.606	1.2	1.374
32	6.638	8.867	7	1.164	1.795
33	7.718	10.479	5.099	2.037	0.333
34	11.42	6.789	7.071	2.098	1.374
35	6.112	10.05	8.062	1.455	1.054
Average	9.961657	7.194629	2.968886	1.244	0.894514

Table 4.3. Approximate sizes of particles from sample 2, obtained using ImageJ

CHAPTER 5

CONCLUSIONS AND FUTURE WORK

5.1 Conclusions

Inertial cascade impactors are tremendously useful to perform industrial hygiene air quality

inspection. Their importance lies in their capability to separate particulate matter by aerodynamic

sizes, giving researchers the possibility to obtain samples that can be easily analyzed in a

laboratory. The results obtained from these samples enable personnel in management positions to

determine the best actions to be taken to reduce the exposure of workers to particulate matter in

their work environment to safe levels. These actions could include to require personnel to wear

specific personal protective equipment, e.g. facemasks, respirators, etc.; to identify and locate

possible contamination sources inside industrial facilities; and to take the respective measures to

eliminate them completely, or to reduce their impact to the minimum permissible to protect

personnel who perform their daily duties in close proximity to them.

Despite their ease of use, assembling, and sample taking, the design inertial cascade impactors

requires an advanced knowledge of the physics that make them function. The objective of this

thesis was to apply the knowledge of fluid dynamics to design this device. It is important to

mention, however, that due to the complexity of the geometry involved, it was necessary to use a

commercial finite element package, COMSOL, to facilitate this process. This software provided

the velocity field representation for a 2D turbulent model, which was solved using the kinetic-

epsilon model. It was observed that the velocity values in the nozzles of each stage calculated

with COMSOL are very close to the values calculated using the Marple-Willeke procedure. This

velocity field also indicated that certain regions of the cascade impactor cavity could be reduced

since not much air motion happens in them. By omitting these regions, less material would be necessary to manufacture the inertial cascade impactor, making it less expensive.

Another important observation was that the images obtained from the samples under the microscope showed that most of the particulate matter was collected in the stages 4 and 5, after conducting the first experiment. By microscopic inspection, it could be seen that these particles were roughly smaller than 1 µm. The upper stages collected bigger particles, which was expected. The collection period for this first sample was 24 hours; however, not much particulate matter as expected was collected during this time. The main cause for this could be them bouncing off the collection paper as soon as it hits it. This issue was reduced in the second experiment by adding a light film of oil to the collection paper, which aided the impinging particles stick to it, instead of bouncing off to reunite with the air flow and continue downstream to the lower stages. Despite this, still some bigger particles were observed in lower stages, but their concentration was smaller. Another possible cause for observing bigger particles in lower stages could be the fact that an initial assumption of particulate matter density of $\rho_p = 1\frac{g}{cm^3}$. Since the sample was taken in an open space, it is not completely accurate to assume this density, however, this is a starting point for designing purposes. Therefore, changes in density also shift the cutoff diameter. Finally, temperature changes can also affect the air density. The first sample was taking during a period of 24 hours during which the temperature fluctuated from low 46º F to 57º F. The second sample was taken during a 60-hour period during which the temperature fluctuated from low 36º F to 70º F. The density of air or design purposes was assumed at standard temperature, which is 68º F.

An important observation was that the average number of particles in each stage are within the expected cutoff diameter, and some variation could be due to bouncing of particles when hitting the collection plates. This was observed mainly in the last stage.

The approximate sizes of the particles were obtained using the software ImageJ to measure the approximate length of several particles from the images captured with the microscope. The sizes of most of the particles observed fell within the expected range in each stage, as shown in Table 4.3. This was an indication of the effectiveness of the designed inertial cascade impactor.

5.2 Future work

The design of the inertial cascade impactor can be improved in several different ways, which requires further application of CFD principles to understand better how changing the geometry of the impactor's cavity would affect the efficiency of this device.

One way to do this is by investigating how the distance from the collection plate edge to the inner wall of each stage affects the fluid flow, and the collection of particulate matter. This could be done by reducing the area of the collection plates. Experiments would help verify the agreement between theoretical, numerical, and experimental studies. Additionally, the same iterative process could be used to model the inlet cone, to determine how changing its geometry could improve the design of the inertial cascade impactor. Additionally, particle trajectory tracing could help understand better how particles behave once they enter the cavity of the inertial cascade impactor

Another improvement to this research work could be the study of wall losses, which could help estimate how much dust does not collect on the collection plates, but in the internal walls on the cascade impactor. This way, a better estimate of the particulate matter concentration in the aerosol sample could be obtained. Particle bouncing could also be studied, and for this purpose, particle trajectory tracing could be implemented using appropriate finite element analysis software, like COMSOL, which was used in this thesis.

Collecting the samples of a cascade impactor requires the device to be stopped and disassembled. This process interrupts the collection process. It would be significant to modify the initial design of the cascade impactor so that the collection of samples could be performed without interrupting

its work. This would probably require a design that incorporates a lateral opening that would open to collect the sample, and then close after retrieving the sample.

Another interesting future work could be varying the flow rate of the vacuum pump by adding a flow rate controller so that the change in cutoff diameter for each stage can be studied theoretically, numerically, and experimentally. Besides, more samples could be taken, and efficiency curves plotted with the data collected.

APPENDIX A

Definitions

Aerodynamic diameter: Applies to irregular-shaped particles and represents the diameter of this particle such that its terminal settling velocity is equal to the settling velocity of a spherical particles with density equal to $1000 \frac{kg}{m^3}$.

Aerosol: An air sample with particulate matter (solid or liquid) in suspension.

Collection efficiency curve: Indicates the percent of particles of any size which are collected on the impaction plate as a function of the particle size (Marple V. A. & Willeke K., 1967).

Inertial cascade impactors: Instruments that separate the particulate matter in aerosol samples by using the inertia of its particles, which depends on a particle's velocity and aerodynamic size.

Mucociliary escalator: A defense mechanism of the human body through which particulate matter is removed from the respiratory system.

Nozzle: Opening through which air flows inside the inertial cascade impactor before impinging on the collection plate in each stage. The y can be rounded or rectangular.

Stokes Number: Ratio of the particle stopping distance to the half-width or the radius of the impactor throat (Marple V. A. & Willeke K., 1967).

$$Stk = \frac{\rho_p V_0 \frac{D_p^2}{18\mu}}{\frac{W}{2}}$$

Terminal settling velocity: Velocity with which particles settle down in the respiratory system.

REFERENCES

Berkenfeld, Bernauer, Mcconville, & Lamprecht. (2018). Investigating cascade impactor performance using a modified 3D printed induction port. *International Journal of Pharmaceutics, 535*(1-2), 402-409.

Çengel Y. A. & Cimbala J. M. (2006). *Fluid mechanics. Fundamentals and applications*. New York, NY: The McGraw-Hill Companies, Inc.

Chan, Vowles, Mctainsh, Simpson, Cohen, Bailey, & Mcorist. (2000). Simultaneous collection of airborne particulate matter on several collection substrates with a high-volume cascade impactor. *Atmospheric Environment, 34*(16), 2645-2651.

Clayton G. & Clayton F. (1991). *Patty's Industrial Hygiene and Toxicology* (4th ed., Volume I). New York, NY: John Wiley & Sons, Inc.

Dechraksa, J., Suwandecha, T., Maliwan, K., & Srichana, T. (2014). The Comparison of Fluid Dynamics Parameters in an Andersen Cascade Impactor Equipped With and Without a Preseparator. *AAPS PharmSciTech, 15*(3), 792-801.

Dunbar, Kataya, & Tiangbe. (2005). Reducing bounce effects in the Andersen cascade impactor. *International Journal of Pharmaceutics, 301*(1), 25-32.

Durst F. (2008). *Fluid mechanics. An introduction to the theory of fluid flows*. Berlin, Germany: Springer-Verlag.

Flynn, Tong, Yang, Kamiya, Yu, & Chan. (2015). Computational fluid dynamics (CFD) investigation of the gas–solid flow and performance of Andersen cascade impactor. *Powder Technology, 285*, 128-137.

Garmise, & Hickey. (2008). Calibration of the Andersen Cascade Impactor for the Characterization of Nasal Products. *Journal of Pharmaceutical Sciences, 97*(8), 3462-3466.

Gulak, Jayjock, Muzzio, Bauer, & Mcglynn. (2009). Numerical calibration of the Andersen cascade impactor using a single jet model. *International Journal of Pharmaceutics, 377*(1), 45-51.

Huang, & Tsai. (2001). Effect of gravity on particle collection efficiency of inertial impactors. *Journal of Aerosol Science, 32*(3), 375-387.

Kamiya, A., Sakagami, M., & Byron, P. (2009). Cascade impactor practice for a high dose dry powder inhaler at 90 L/min: NGI versus modified 6-stage and 8-stage ACI. *Journal of Pharmaceutical Sciences, 98*(3), 1028-1039.

Kwon, Kim, & Lee. (2002). Effects of jet configuration on the performance of multi-nozzle impactors. *Journal of Aerosol Science, 33*(6), 859-869.

Kwon, Lim, Jung, Bae, & Lee. (2003). Design and calibration of a 5-stage cascade impactor (K-JIST cascade impactor). *Journal of Aerosol Science, 34*(3), 289-300.

Lee, C., Lee, Y. H., Park, S. H., & Lee, K. W. (2006). Design and Evaluation of Four-Stage Low-Pressure Cascade Impactor Using Electrical Measurement System. *Particulate Science and Technology, 24*(3), 329-351.

Liu, Awasthi, & Tsai. (2012). Collection efficiency and interstage loss of nanoparticles in micro-orifice-based cascade impactors. *Atmospheric Environment,* Atmospheric Environment.

Marple V. A. (1970). Ph.D. thesis, University of Minnesota.

Marple, Liu, & Kuhlmey. (1981). A uniform deposit impactor. *Journal of Aerosol Science, 12*(4), 333-337.

Marple, Liu, & Whitby. (1974). Fluid mechanics of the laminar flow aerosol impactor. *Journal of Aerosol Science, 5*(1), 1, IN1, 5-4, IN1, 16.

Marple V. A. & Willeke K. (1967). Impactor Design. *Atmospheric Environment*, 10(10), 891-896

Mercer, & Chow. (1968). Impaction from rectangular jets. *Journal of Colloid And Interface Science, 27*(1), 75-83.

Mercer, Tillery & Newton G. (1970). A multi-stage, low flow rate cascade impactor. Journal of Aerosol Science, 1(1), 9-15.

Newton, Raabe, & Mokler. (1977). Cascade impactor design and performance. *Journal of Aerosol Science, 8*(5), 339-347.

Pennanen, Sillanpää, Hillamo, Quass, John, Branis, . . . Salonen. (2007). Performance of a high-volume cascade impactor in six European urban environments: Mass measurement and chemical characterization of size-segregated particulate samples. *Science of the Total Environment, 374*(2), 297-310.

Picknett, R. (1972). A new method of determining aerosol size distributions from multistage sampler data. *Journal of Aerosol Science, 3*(3), 185-198.

Plog B. & Quinlan P. (2012). *Fundamentals of Industrial Hygiene* (6th ed.). Itaca, IL: National Safety Council.

Roberts, D., & Mitchell, L. (2013). The Effect of Nonideal Cascade Impactor Stage Collection

  Efficiency Curves on the Interpretation of the Size of Inhaler-Generated Aerosols. *AAPS*

  PharmSciTech, 14(2), 497-510.

Roberts, D., & Mitchell, L. (2019). Measurement of Aerodynamic Particle Size Distribution of

  Orally Inhaled Products by Cascade Impactor: How to Let the Product Specification

  Drive the Quality Requirements of the Cascade Impactor. *AAPS PharmSciTech, 20*(2), 1-

  10.

Rosenhead L. (1963). *Laminar boundary layers*. Great Britain: Oxford University Press.

Schlichting H. & Gersten K. (2017). *Boundary-Layer Theory* (9th ed.)*.* Berlin: Springer.

Singh, Misra, & Sioutas. (2003). Field evaluation of a personal cascade impactor sampler

  (PCIS). *Atmospheric Environment, 37*(34), 4781-4793.

Singh, Sapra, Khan, Kothalkar, & Mayya. (2010). Development of a variable configuration

  cascade impactor for aerosol size distribution measurement. *Atmospheric*

  Environment, 44(6), 795-802.

Sioutas, Ferguson, Wolfson, Ozkaynak, & Koutrakis. (1997). Inertial collection of fine particles

  using a high-volume rectangular geometry conventional impactor. *Journal of Aerosol*

  Science, 28(6), 1015-1028.

Srichana, Martin, & Marriott. (1998). Calibration method for the andersen cascade

  impactor. *Journal of Aerosol Science, 29*, S761-S762.

Vaughan, N. (1989). The Andersen impactor: Calibration, wall losses and numerical simulation. *Journal of Aerosol Science, 20*(1), 67-90.

Vinchurkar, Longest, & Peart. (2009). CFD simulations of the Andersen cascade impactor: Model development and effects of aerosol charge. *Journal of Aerosol Science, 40*(9), 807-822.

Weber, B., Lee, S., Delvadia, L., Lionberger, R., Li, R., Tsong, B., & Hochhaus, V. (2015). Application of the Modified Chi-Square Ratio Statistic in a Stepwise Procedure for Cascade Impactor Equivalence Testing. *The AAPS Journal, 17*(2), 370-379.

Wu, Y., & Vincent, J. (2007). A Modified Marple-Type Cascade Impactor for Assessing Aerosol Particle Size Distributions in Workplaces. *Journal of Occupational and Environmental Hygiene, 4*(10), 798-807.

Yoshida, H., Kuwana, A., Shibata, H., Izutsu, K., & Goda, Y. (2017). Comparison of Aerodynamic Particle Size Distribution Between a Next Generation Impactor and a Cascade Impactor at a Range of Flow Rates. *AAPS PharmSciTech, 18*(3), 646-65

VITA

Hector J. Gortaire

EDUCATION

Master of Science in Aerospace Engineering at Old Dominion University, August 2017 – present. Thesis title: "Design and manufacture of an inertial cascade impactor for industrial hygiene purposes".

Bachelor of Science (May 2016) in Aerospace Engineering, Old Dominion University, Norfolk, Virginia.

PROFESSIONAL MEMBERSHIP

American institute of Aeronautics and Astronautics (AIAA).